New Journal of Physics
The open access journal at the forefront of physics
Deutsche Physikalische Gesellschaft DPG IOP Institute of Physics

PAPER • OPEN ACCESS

Theory of wetting dynamics with surface binding

To cite this article: Xueping Zhao *et al* 2024 *New J. Phys.* **26** 103025

IOP Publishing New J. Phys. 26 (2024) 103025 https://doi.org/10.1088/1367-2630/ad80bb

New Journal of Physics

The open access journal at the forefront of physics

Deutsche Physikalische Gesellschaft DPG
IOP Institute of Physics

Published in partnership with: Deutsche Physikalische Gesellschaft and the Institute of Physics

CrossMark

OPEN ACCESS

RECEIVED
27 February 2024

REVISED
21 September 2024

ACCEPTED FOR PUBLICATION
27 September 2024

PUBLISHED
23 October 2024

PAPER

Theory of wetting dynamics with surface binding

Xueping Zhao[1], **Susanne Liese**[2], **Alf Honigmann**[3,4,7], **Frank Jülicher**[4,5,6,*] and **Christoph A Weber**[2,*]

[1] Department of Mathematical Sciences, University of Nottingham Ningbo China, Taikang East Road 199, Ningbo, 315104, People's Republic of China
[2] Faculty of Mathematics, Natural Sciences, and Materials Engineering: Institute of Physics, University of Augsburg, Universitätsstr. 1, Augsburg, 86159, Germany
[3] Biotechnology Centre (BIOTEC), TU-Dresden, Tatzberg 47, Dresden, 01307, Germany
[4] Cluster of Excellence Physics of Life, TU Dresden, Arnoldstraße 18, Dresden, 01307, Germany
[5] Max Planck Institute for the Physics of Complex Systems, Nöthnitzer Strasse 38, Dresden, 01187, Germany
[6] Center for Systems Biology Dresden, Pfotenhauerstrasse 108, Dresden, 01307, Germany
[7] Max Planck Institute of Molecular Cell Biology and Genetics, Pfotenhauerstrasse 108, Dresden, 01307, Germany
[*] Authors to whom any correspondence should be addressed.

E-mail: julicher@pks.mpg.de and christoph.weber@physik.uni-augsburg.de

Keywords: liquid–liquid phase separation, surface binding, wetting, non-equilibrium thermodynamics, biomolecular condensates

Abstract

Biomolecules, such as proteins and nucleic acids, can phase separate in the cytoplasm of cells to form biomolecular condensates. Such condensates are often liquid-like droplets that can wet biological surfaces such as membranes. Many molecules that participate in phase separation can also reversibly bind to membrane surfaces. When a droplet wets a surface, molecules can diffuse inside and outside of the droplet or in the bound state on the surface. How the interplay between surface binding, diffusion in surface and bulk affects the wetting kinetics is not well understood. Here, we derive the governing equations using non-equilibrium thermodynamics by relating the thermodynamic fluxes and forces at the surface coupled to the bulk. We study the spreading dynamics in the presence of surface binding and find that binding speeds up wetting by nucleating a droplet inside the surface. Our results suggest that the wetting dynamics of droplets can be regulated by two-dimensional surface droplets in the surface-bound layer through changing the binding affinity to the surfaces. These findings are relevant both to engineering life-like systems with condensates and vesicles, and biomolecular condensates in living cells.

1. Introduction

Living cells organize their chemical reactions in space by forming various compartments. These compartments provide different chemical environments for distinct biochemical processes. Some compartments are bounded by a membrane surface composed of lipids and proteins. Examples are the nucleus [1], endoplasmic reticulum, golgi apparatus, mitochondria [2], plastids, lysosomes [3] and endosomes. However, many compartments in cells have no membrane as boundaries. Examples include the nucleolus [4], centrosomes [5], Cajal bodies [6], P granules [7, 8], and stress granules [9, 10]. These membrane-less organelles, termed biomolecular condensates, often behave as liquid-like droplets formed in a process similar to liquid–liquid phase separation [4, 7, 8].

Biomolecular condensates can attach to biological surfaces such as membranes. This process is referred to as wetting. Examples are P granules wetting on the surface of the nucleus [7], or TIS granules wetting the endoplasmic reticulum [11]. Furthermore, many biological molecules that phase separate can also bind to biological surfaces, leading to a two-dimensional molecular layer on the surface. The molecules in such surface layers can give rise to rich spatio-temporal patterns. For example, the PAR proteins bind and unbind to the surface periodically, leading to asymmetrical localization during the asymmetric cell division [12, 13]. The *Escherichia-coli* MinCDE system is another example of pattern formation in the surface layer of bound molecule layer [14]. Molecules bound to surfaces can also nucleate the formation of biomolecular condensates in the bulk. An example is Sec bodies induced by amino-acid starvation in Drosophila cells where small condensate nuclei form at the endoplasmic reticulum's exit sites (ERESs) [15].

The relevance of surface binding and clustering for surface phase transitions such as surface phase separation and prewetting was studied at thermodynamic equilibrium [16–18]. A key finding is that the prewetting transition can occur far below the equilibrium concentration and is accessible for a larger range of thermodynamic parameters as compared to the case without surface binding. Zhao *et al* [16] also showed that the interplay between surface-bound molecules and free diffusive molecules in the bulk can also lead to multiple pre-wetted states. Interestingly, binding also shifts the wetting transition line and affects the contact angle. These phenomena rely on surface binding, effectively modifying the properties of the surface for prewetting and wetting. The idea of modifying surface properties to affect wetting was also explored in systems undergoing reactive [19, 20] or adaptive wetting [21].

The droplet dynamics of wetting have been described using a fluid dynamical model based on viscous dissipation and a transition state model describing the contact line motion as adsorption and desorption kinetics [22, 23]. The dynamics toward a completely wetted state are governed by Tanner's law [23, 24], where the contact angle exhibits a power-law relaxation in time t toward thermodynamic equilibrium, $\theta \propto t^{-3/10}$. This law implies very slow spreading dynamics of the droplet contact area proportional to $t^{1/5}$. Tanner's law and the dynamics of the contact area require a *nm*-thick precursor film on which the droplet spreads [25–28]. The film extends from the droplet further out and grows with the wetting droplet. In biological systems, such a film of molecular thickness could form via the binding of molecules from the liquid bulk domains to the adjacent biological surfaces. Despite the significance of wetting and molecular binding in biological systems [18, 29], the exploration of the dynamics of wetting in conjunction with surface binding, remains largely unexplored.

To bridge this gap, we have derived the governing dynamic equations of a bulk droplet wetting a surface where droplet molecules can bind. To this end, we use irreversible thermodynamics. Moreover, we developed a two-dimensional numerical solver to explore the effects of surface binding on the dynamics of wetting. We show that surface binding speeds up the dynamics of droplet spreading by orders in magnitude depending on the binding rate coefficient. Our findings indicate that surface binding can act as a switch to control the wetting of droplets in living cells.

This paper is structured as follows: In section 2, we derive the model for phase separation in bulk and surface coupled by surface binding using irreversible thermodynamics. Section 3 is devoted to an application of the developed dynamic model: We discuss spreading to a completely wetted state and spreading toward a partially wetted state. Finally, in section 4, we present our conclusions and outline potential future directions based on our findings.

2. Non-equilibrium thermodynamics of wetting with surface binding

We consider a binary mixture in a three-dimensional domain V that we refer to as the bulk in the following. The bulk is coupled to a two-dimensional surface S. We describe the system using a canonical ensemble where temperature T, the size of the volume $|V|$ and surface area $|S|$, as well as the total particle number N in bulk and surface are fixed. For simplicity, the bulk is a cubic volume $|V| = L^3$, where L is the side length. The molecules in the bulk can bind to the lower surface S of the cubic volume, which we refer to as the binding surface. The remaining non-binding and non-interacting surfaces of the cubic volume are denoted by ∂V; see figure 1(a) for a sketch. The molecules in the bulk domain V diffuse, bind to, and unbind from the surface S, leading to a layer of bound molecules. Molecules in this layer can only diffuse on the surface. We consider an incompressible system in bulk and surface, respectively. Thus, we can describe the wetting dynamics depicted in figures 1(b) and (c) using bulk volume fraction $\phi(\boldsymbol{x},t)$ of the molecules and their area fraction bound to the surface, $\phi_s(\boldsymbol{x}_\parallel,t)$. Here, $\boldsymbol{x} = (x,y,z)$ is the bulk position and $\boldsymbol{x}_\parallel = (x,y)$ the position in the surface. The surface is located at $z = 0$.

2.1. Conservation laws

The dynamics of the bulk volume fraction ϕ and the area fraction ϕ_s are governed by conservation laws expressed for surface and bulk:

$$\partial_t \phi = -\nabla\cdot\boldsymbol{j}\,, \qquad \boldsymbol{x}\in V\,, \tag{1a}$$

$$\partial_t \phi_s = -\nabla_\parallel\cdot\boldsymbol{j}_s + r\,, \qquad \boldsymbol{x}\in S\,, \tag{1b}$$

where $\boldsymbol{j}$ and $\boldsymbol{j}_s$ are the diffusive fluxes in bulk and surface. Moreover, r denotes the binding flux. Particle conservation relates the binding flux r to the normal component of the diffusive flux $\boldsymbol{j}$ at the surface

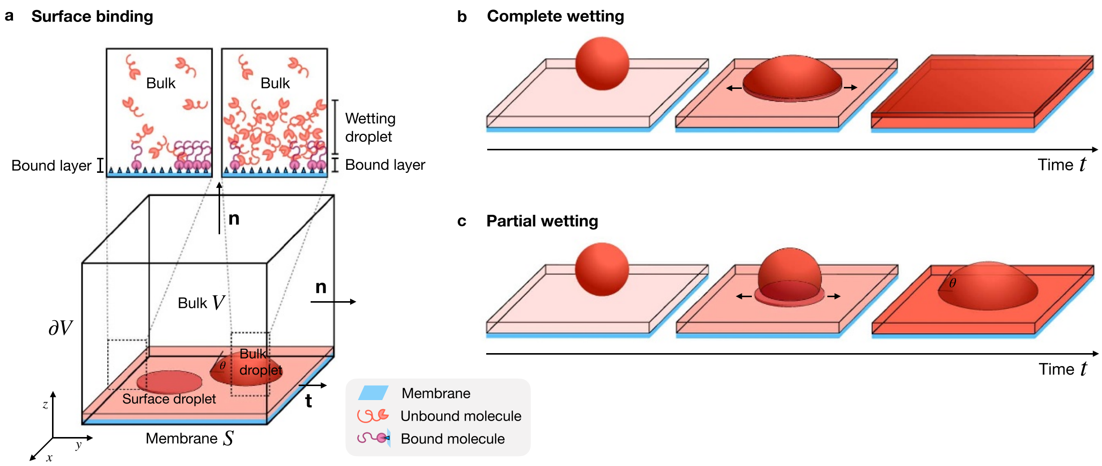

Figure 1. Schematics of wetting dynamics on binding surfaces. (a) A binary mixture in bulk and surface is shown to be coupled by interactions and surface binding. The bulk mixture can phase separate and give rise to a bulk droplet. Binding builds up a molecular layer of bound molecules that can phase-separate, leading to a surface droplet. We consider a planar binding surface S and a cubic bulk domain V. The non-interacting and non-binding surfaces are denoted as ∂V. Wetting of the bulk droplet on the surface is characterized by the contact angle θ. (b) and (c) Schematic of the spreading dynamics of a bulk droplet towards a completely wetted or partially wetted thermodynamic equilibrium state.

(derivation see appendix A):

$$\boldsymbol{n}\cdot\boldsymbol{j} = r\frac{\nu}{\nu_s}\,,\qquad \boldsymbol{x}\in S\,, \tag{1c}$$

where ν and ν_s denote the molecular volume and molecular area, and $\boldsymbol{n}$ denotes the surface normal pointing outward of the volume domain V; see figure 1. As molecules cannot bind or interact with the remaining boundaries ∂V, the flux normal to the surface vanishes:

$$\boldsymbol{n}\cdot\boldsymbol{j} = 0\,,\qquad \boldsymbol{x}\in \partial V\,. \tag{1d}$$

Alternatively, for the ∂V boundaries that are not opposite to the binding surface S, periodic boundaries could be considered. We also have to impose the conditions at the one-dimensional boundary lines of the binding surface S, which we denote as ∂S. To conserve volume, periodic boundary conditions could be imposed or $\boldsymbol{t}\cdot\boldsymbol{j}_s = 0$, where $\boldsymbol{t}$ is the normal to the one-dimensional boundary ∂S; see figure 1. The dynamic equations and boundary conditions above conserve the total particle number N in bulk and in the surface,

$$N = \frac{|V|}{\nu}\bar{\phi} + \frac{|S|}{\nu_s}\bar{\phi}_s\,, \tag{2}$$

where

$$\bar{\phi}(t) = |V|^{-1}\int_V \mathrm{d}V\phi(\boldsymbol{x},t) \tag{3}$$

is the average bulk volume fraction and

$$\bar{\phi}_s(t) = |S|^{-1}\int_S \mathrm{d}S\,\phi_s(\boldsymbol{x}_\parallel,t) \tag{4}$$

is the average area fraction. Moreover, $|V|$ is the volume of the bulk, and $|S|$ is the surface area of the surface to which the molecules bind.

The fluxes $\boldsymbol{j}$, $\boldsymbol{j}_s$, and r are driven by the conjugate thermodynamic forces. These relationships are derived in section 2.4 using irreversible thermodynamics. Since the thermodynamic forces are non-linear in the field $\phi(x,t)$ and $\phi_s(x,t)$, we employ numerical methods to solve the non-linear dynamic equations.

2.2. Free energy

The free energy governs interactions among components in bulk and surface. The total Helmholtz free energy $F[\phi,\phi_s]$ depends on the two independent thermodynamic fields $\phi(\boldsymbol{x},t)$ and $\phi_s(\boldsymbol{x}_\parallel,t)$ and their spatial derivatives. It can be decomposed into four parts: the bulk free energy density $f(\phi)$, the surface free energy density $f_s(\phi_s)$, the coupling free energy density between bulk and surface $J(\phi|_{z=0},\phi_s)$, and free energy costs for gradients of the bulk volume fraction parallel to the surface:

$$\begin{aligned} F[\phi,\phi_s] = &\int_V \mathrm{d}V \left[f(\phi) + \frac{1}{2}\kappa(\nabla\phi)^2\right] \\ &+ \int_S \mathrm{d}S \left[f_s(\phi_s) + \frac{1}{2}\kappa_s\left(\nabla_\parallel\phi_s\right)^2 + J\left(\phi_s,\phi|_{z=0}\right) + \frac{1}{2}\kappa_0\left(\nabla_\parallel\phi|_{z=0}\right)^2\right], \end{aligned} \tag{5}$$

where $\phi(\boldsymbol{x}_\parallel,t)|_{z=0} = \phi(x,y,z,t)|_{z=0}$ is the bulk volume fraction at the surface, and $\mathrm{d}V = \mathrm{d}x\mathrm{d}y\mathrm{d}z$ and $\mathrm{d}S = \mathrm{d}x\mathrm{d}y$ are the volume and surface elements for the considered cubic system. The free energy costs due to gradients in volume fraction in bulk and at the surface are characterized by the coefficients κ, κ_0, respectively, while in the bound layer, the correspondingly parameter is κ_s. Moreover, $\nabla_\parallel = (\partial_x,\partial_y)$ denotes the gradient vector in the x–y surface plane.

Before we derive the diffusive fluxes $\boldsymbol{j}$ and $\boldsymbol{j}_s$ and the binding flux r using irreversible thermodynamics in section (2.4), we determine the conditions for thermodynamic equilibrium as a reference in the next section.

2.3. Thermodynamic equilibrium

At thermodynamic equilibrium and for a T-V-N ensemble, the total Helmholtz free energy F is minimal with the binding constraint of the total molecule number N (equation (2)) being conserved:

$$0 = \delta\left(F[\phi,\phi_s] - \lambda\left[\int_V \mathrm{d}V\,\phi/\nu + \int_S \mathrm{d}S\,\phi_s/\nu_s - N\right]\right), \tag{6}$$

where δ denotes a variation and λ is the Lagrange multiplier fixing N. Using equation (5), the variation of the total Helmholtz free energy is given as:

$$\begin{aligned} \delta F = &\int_V \mathrm{d}V\left(f'(\phi) - \kappa\nabla^2\phi\right)\delta\phi \\ &+ \int_S \mathrm{d}S\left[\left(f_s'(\phi_s) - \kappa_s\nabla_\parallel^2\phi_s + \frac{\partial J}{\partial\phi_s}\right)\delta\phi_s + \left(\frac{\partial J}{\partial\phi|_{z=0}} - \kappa_0\nabla_\parallel^2\phi|_{z=0} + \boldsymbol{n}\cdot\kappa\left(\nabla\phi\right)|_{z=0}\right)\delta\phi|_{z=0}\right] \\ &+ \int_{\partial V} \mathrm{d}S\left(\boldsymbol{n}\cdot\kappa\left(\nabla\phi\right)\right)\delta\phi|_{\partial V} + \int_{\partial S} \mathrm{d}l\left(\boldsymbol{t}\cdot\kappa_s\nabla_\parallel\phi_s\right)\delta\phi_s, \end{aligned} \tag{7}$$

where ∂S is the one-dimensional boundary of the surface S and $\boldsymbol{t}$ is the normal vector to this boundary.

We identify five thermodynamic forces related to deviations of the independent fields ϕ and ϕ_s in the respective spatial domains. Following equation (7), we define the exchange chemical potentials for the bulk, μ, exchange chemical potentials for the binding to the surface, μ_s, and the chemical potential for the surface of the bulk boundary, μ_0:

$$\mu = \nu\frac{\delta F}{\delta\phi} = \nu\left(f'(\phi) - \kappa\nabla^2\phi\right) \tag{8a}$$

$$\mu_s = \nu_s\frac{\delta F}{\delta\phi_s} = \nu_s\left(f_s'(\phi_s) - \kappa_s\nabla_\parallel^2\phi_s + \frac{\partial J}{\partial\phi_s}\right), \tag{8b}$$

$$\mu_0 = \nu_s\frac{\delta F}{\delta\phi|_{z=0}} = \nu_s\left(\frac{\partial J}{\partial\phi|_{z=0}} - \kappa_0\nabla_\parallel^2\phi|_{z=0} + \boldsymbol{n}\cdot\kappa\left(\nabla\phi\right)|_{z=0}\right), \tag{8c}$$

where the prime denotes a derivative, e.g. $f'(\phi) = \mathrm{d}f/\mathrm{d}\phi$. The bulk chemical potential μ is related to variations of the volume fraction in the bulk, $\delta\phi$, the surface chemical potential μ_s to variations of the area fraction of bound molecules, $\delta\phi_s$, and μ_0 to variations of the bulk volume fraction at $z=0$ at the binding surface S, $\delta\phi|_{z=0}$. Similarly, $\boldsymbol{n}\cdot\kappa\left(\nabla\phi\right)|_{z=0}$ is the thermodynamic force associated with deviations of bulk volume fraction at the non-interacting and non-binding surface ∂V, $\delta\phi|_{\partial V}$. Finally, $\boldsymbol{t}\cdot\kappa_s\nabla_\parallel\phi_s$ is a thermodynamic force when perturbing ϕ_s at the boundary of S, denoted as ∂S. We note that the bulk chemical potential evaluated at $z=0$ is different from the chemical potential for the surface of the bulk boundary μ_0 ($\mu|_{z=0} \neq \mu_0$).

All five thermodynamic forces characterize the work performed when varying one of the concentration fields in a specific spatial domain. When changing this field away from its equilibrium value, dissipation occurs and entropy is produced, which we discuss in detail in the next section on irreversible thermodynamics 2.4.

The entire system composed of surface and bulk is at thermodynamic equilibrium if condition (6) is satisfied. This condition implies that the surface and bulk exchange chemical potentials are constant and equal to the Lagrange multiplier,

$$\lambda = \mu_s = \mu \,. \tag{9a}$$

Moreover,

$$\mu_0 = 0\,, \tag{9b}$$

and at the surface S and the other non-binding and non-interacting surfaces ∂V of the volume V, the following boundary conditions are fulfilled:

$$\kappa\, \boldsymbol{n}\cdot(\nabla\phi)\,|_{\partial V} = 0\,, \qquad \boldsymbol{x}\in\partial V\,, \tag{9c}$$

$$\kappa_s\, \boldsymbol{t}\cdot\nabla_{||}\phi_s = 0\,, \qquad \boldsymbol{x}\in\partial S\,. \tag{9d}$$

Note the ∂V boundaries are termed 'non-interacting' since the coupling free energy density J vanishes at such boundaries. They are also called 'non-binding' because either the flux normal to ∂V vanishes (equation (1d)) or periodic conditions are considered at ∂V.

The boundary conditions equations (9b)–(9d) are related to the contact angle θ which is defined in the limit of a sharp interface [30]. In this limit, the width of the interface profile ℓ is short compared to the size of the droplet. Local equilibrium implies that the volume fractions at the interface in the molecule-rich (I) and poor (II) phase take the equilibrium values ϕ^{I} and ϕ^{II}, respectively. In the limit of a sharp interface, the gradient of the volume fraction is aligned with the normal to the interface, and we can write $\cos(\theta) = (\boldsymbol{n}\cdot\nabla\phi)\,\ell/(\phi^{\mathrm{I}}-\phi^{\mathrm{II}})$, with the interface width ℓ. The decay of ϕ around the interface is characterized by the length scale $w = \sqrt{\kappa\nu/((\chi-2)k_bT)}$ [31] and we approximate the interface width as $\ell = 3w$, such that it is consistent with the law of Young–Dupré. Using equation (9b), we get a relationship between the contact angle θ and the coupling free energy J:

$$\cos(\theta) = -\frac{\ell}{\kappa\,(\phi^{\mathrm{I}}-\phi^{\mathrm{II}})}\frac{\partial J}{\partial\phi}\,. \tag{10}$$

Accordingly, $J = 0$ corresponds to a contact angle of $\pi/2$, in accordance with the law of Young–Dupré, which gives $\cos(\theta) = 0$ if the surface tensions between the substrate and the molecule-poor or rich phase are identical [16, 32–34]. Thus, the bulk droplet makes a contact angle $\pi/2$ at the non-interacting and non-binding surface ∂V (equation (9c)). Analogously, inside the surface, the boundary condition (9d) implies that surface droplets have a zero contact angle at the surface boundary ∂S.

If the exchange chemical potentials between bulk and surface are not balanced, and/or one of the boundary conditions above is not fulfilled (equations (9)), there will be diffusive fluxes in bulk and surface, $\boldsymbol{j}$ and $\boldsymbol{j}_s$, and a non-zero binding flux r. In this case, the system is out of equilibrium. If the system is not maintained away from equilibrium [31], it relaxes toward thermodynamic equilibrium. During this relaxation, entropy is produced until thermodynamic equilibrium is established. In the following section, we will consider the production of entropy to derive the relationships between the generalized fluxes and their conjugate thermodynamic forces using Onsager linear response.

2.4. Irreversible thermodynamics

In an isothermal system, the rate of change of the system entropy S is proportional to the negative change in the total Helmholtz free energy, $T\dot{S} = -\dot{F}$ [35], where the dot indicates a total time derivative. This change in total free energy can be expressed in terms of the free energy densities by using equation (5):

$$\begin{aligned} T\dot{S} = &-\int_V \mathrm{d}V\,\partial_t\left[f(\phi)+\frac{1}{2}\kappa\,(\nabla\phi)^2\right] \\ &-\int_S \mathrm{d}S\,\partial_t\left[f_s(\phi_s)+\frac{1}{2}\kappa_s\,(\nabla_{||}\phi_s)^2 + J(\phi_s,\phi|_{z=0}) + \frac{1}{2}\kappa_0\,(\nabla_{||}\phi|_{z=0})^2\right] \\ &-\int_{\partial V}\mathrm{d}S\,\boldsymbol{n}\cdot\boldsymbol{j}_{\mathrm{r}1} - \int_{\partial S}\mathrm{d}l\,\boldsymbol{t}\cdot\boldsymbol{j}_{\mathrm{r}2}\,, \end{aligned} \tag{11}$$

where the non-dissipative free energy fluxes through the boundaries of bulk and surface are $\boldsymbol{j}_{r1} = \boldsymbol{j}\mu/\nu$ and $\boldsymbol{j}_{r2} = \boldsymbol{j}_s\mu_s/\nu_s$, respectively.

The entropy production rate can be rewritten using the conservation laws and the boundary conditions (equations (1)) together with the chemical potentials defined in equations (8):

$$T\dot{S} = -\int_V \mathrm{d}V\,(\nabla\mu\cdot\boldsymbol{j}/\nu) \\ -\int_S \mathrm{d}S\,[\nabla_{\|}\mu_s\cdot\boldsymbol{j}_s/\nu_s + (\mu_s - \mu|_{z=0})\,r/\nu_s] - \int_S \mathrm{d}S\,[\mu_0\,\partial_t\phi|_{z=0}/\nu_s] \\ -\int_{\partial V} \mathrm{d}S\,[(\boldsymbol{n}\cdot\kappa\,(\nabla\phi))\,\partial_t\phi|_{\partial V}] - \int_{\partial S} \mathrm{d}l\,\left(\boldsymbol{t}\cdot\kappa_s\nabla_{\|}\phi_s\right)\partial_t\phi_s - \int_{\partial S} \mathrm{d}l\,\left(\boldsymbol{t}\cdot\kappa_0\nabla_{\|}\phi|_{z=0}\right)\partial_t\phi|_{z=0}\,. \tag{12}$$

Using irreversible thermodynamics [36, 37], we identify the following pairs of conjugate thermodynamic fluxes and forces:

$$\boldsymbol{j} \longleftrightarrow -\nabla\mu\,, \qquad \boldsymbol{x}\in V, \tag{13a}$$
$$\boldsymbol{j}_s \longleftrightarrow -\nabla_{\|}\mu_s\,, \qquad \boldsymbol{x}\in S, \tag{13b}$$
$$r \longleftrightarrow -(\mu_s - \mu|_{z=0})\,, \qquad \boldsymbol{x}\in S, \tag{13c}$$
$$\partial_t\phi|_{z=0} \longleftrightarrow -\mu_0\,, \qquad \boldsymbol{x}\in S\,, \tag{13d}$$
$$\partial_t\phi|_{\partial V} \longleftrightarrow -(\boldsymbol{n}\cdot\kappa\nabla\phi)\,, \qquad \boldsymbol{x}\in \partial V, \tag{13e}$$
$$\partial_t\phi_s \longleftrightarrow -\left(\boldsymbol{t}\cdot\kappa_s\nabla_{\|}\phi_s\right)\,, \qquad \boldsymbol{x}\in \partial S. \tag{13f}$$

Here, the quantities in the left column (e.g. $\boldsymbol{j}, \boldsymbol{j}_s, r, \partial_t\phi|_{z=0}$) represent thermodynamic fluxes, whereas those in the right column (e.g. $-\nabla\mu$, $-\nabla_{\|}\mu_s$, $-(\mu_s-\mu|_{z=0})$, $-\mu_0$) denote the corresponding thermodynamic forces, as introduced in section 2.3. The fluxes in the bulk and surface, $\boldsymbol{j}$ and $\boldsymbol{j}_s$, are driven by the respective chemical potential gradients in bulk and surface, $\nabla\mu$ and $\nabla\mu_s$ (equations (13a) and (13b)). The binding rate r results from the chemical potential difference between the surface and bulk chemical potential at to the surface, $(\mu_s - \mu|_{z=0})$ (equation (13c)). Similarly, changes in the bulk volume at the surface, $\partial_t\phi|_{z=0}$, arise due to a mismatch of the chemical potential contributions related to the coupling free energy, $\partial J/\partial\phi|_{z=0}$, and the respective gradient free energy contributions characterized by the parameters κ_0 and κ. At the non-interacting and non-binding surfaces ∂V, the dynamics relaxes toward a neutral boundary with $\boldsymbol{n}\cdot\kappa\nabla\phi = 0$. Similarly, at the line boundary of the binding surface, ∂S, the surface-bound fraction relaxes to $\boldsymbol{t}\cdot\kappa_s\nabla_{\|}\phi_s = 0$.

To linear order, we obtain the following relationships between thermodynamic fluxes and forces:

$$\boldsymbol{j} = -\Lambda\,\nabla\mu\,, \qquad \boldsymbol{x}\in V, \tag{14a}$$
$$\boldsymbol{j}_s = -\Lambda_s\,\nabla_{\|}\mu_s\,, \qquad \boldsymbol{x}\in S, \tag{14b}$$
$$r = -\Lambda_r\,(\mu_s - \mu|_{z=0}) - \Lambda_{r\kappa}\,\mu_0\,, \qquad \boldsymbol{x}\in S, \tag{14c}$$
$$\partial_t\phi|_{z=0} = -\Lambda_{r\kappa}\,(\mu_s - \mu|_{z=0}) - \Lambda_\kappa\,\mu_0\,, \qquad \boldsymbol{x}\in S, \tag{14d}$$
$$\partial_t\phi|_{\partial V} = -\Lambda_\kappa\,(\boldsymbol{n}\cdot\kappa\nabla\phi)\,, \qquad \boldsymbol{x}\in \partial V, \tag{14e}$$
$$\partial_t\phi_s = -\Lambda_{\kappa_s}\,\left(\boldsymbol{t}\cdot\kappa_s\nabla_{\|}\phi_s\right)\,, \qquad \boldsymbol{x}\in \partial S. \tag{14f}$$

All the fluxes above ensure that the entropy of the system increases when the system approaches thermodynamic equilibrium. In other words, linear relationship above are consistent with the second law of thermodynamics. Here, $\Lambda > 0$ and $\Lambda_\alpha > 0$ $(\alpha = r, r\kappa, \kappa, \kappa_s)$ denote positive kinetic coefficients, i.e. mobilities or rate coefficients. Specifically, Λ and Λ_s are the diffusive Onsager mobilities for bulk and surface, and Λ_r is the Onsager coefficient for surface binding. Moreover, Λ_κ and Λ_{κ_s} are Onsager coefficients that govern the relaxation time toward the equilibrium boundary conditions (9b)–(9d). Due to Onsager's reciprocal relationship and when considering linear irreversible thermodynamics, there is only one Onsager cross-coupling denoted as $\Lambda_{r\kappa}$.

2.5. Dynamic equations

In summary, full dynamic equations for the bulk V and the binding surfaces S are:

$$\partial_t\phi = \nabla\cdot(\Lambda\nabla\mu)\,, \qquad \boldsymbol{x}\in V, \tag{15a}$$
$$\partial_t\phi_s = \nabla_{\|}\cdot\left(\Lambda_s\nabla_{\|}\mu_s\right) + r\,, \qquad \boldsymbol{x}\in S, \tag{15b}$$

with binding flux given as

$$r = -\Lambda_r \left(\mu_s - \mu|_{z=0}\right) - \Lambda_{r\kappa}\,\mu_0\,. \tag{15c}$$

The chemical potentials depend on the two fields $\phi(\boldsymbol{x},t)$ and $\phi_s(\boldsymbol{x}_{\|},t)$ (and gradients thereof) and are given in equations (8). Equations (15*a*) and (15*b*) are partial differential equations of 4th order requiring two conditions at each boundary domain, i.e. at the binding surface S and the non-binding and non-interacting ∂V, respectively, and at ∂S:

$$\partial_t\phi|_{z=0} = -\Lambda_{r\kappa}\left(\mu_s - \mu|_{z=0}\right) - \Lambda_\kappa\,\mu_0\,, \qquad \boldsymbol{x}\in S\,, \tag{15d}$$

$$-\boldsymbol{n}\cdot\left(\Lambda\nabla\mu\right) = r\frac{\nu}{\nu_s}\,, \qquad \boldsymbol{x}\in S\,, \tag{15e}$$

$$\partial_t\phi|_{\partial V} = -\Lambda_\kappa\left(\boldsymbol{n}\cdot\kappa\nabla\phi\right)\,, \qquad \boldsymbol{x}\in\partial V\,, \tag{15f}$$

$$-\boldsymbol{n}\cdot\left(\Lambda\nabla\mu\right) = 0\,, \qquad \boldsymbol{x}\in\partial V\,, \tag{15g}$$

$$\partial_t\phi_s = -\Lambda_{\kappa_s}\left(\boldsymbol{t}\cdot\kappa_s\nabla_{\|}\phi_s\right)\,, \qquad \boldsymbol{x}\in\partial S\,, \tag{15h}$$

with the second boundary condition at ∂S either being periodic or $\boldsymbol{t}\cdot\nabla\mu_s = 0$. The total number of molecules N is conserved during the binding dynamics between the bulk domain V and S which is ensured by the boundary conditions (15*e*). Please note that the right hand sides of equations (15*d*), (15*f*) and (15*h*) are not sink or source terms; they describe the relaxation toward equilibrium and cause the accumulation of molecules at the respective domain boundary.

At binding equilibrium $\mu_s = \mu|_{z=0}$ and when decoupling the surface and bulk components (i.e. $\Lambda_{r\kappa} = 0$ and $\chi_{0s} = 0$), the equations above simplify to the classical Cahn–Hilliard equation (equation (15*a*)) with dynamic boundary conditions (equations (15*d*) and (15*g*)), as described in [38–40].

The bulk chemical potential in bulk μ and the surface chemical potential μ_s contain the derivatives of the bulk free energy densities $f'(\phi)$ and surface free energy densities $f_s'(\phi_s)$ (equations (8)), respectively, which correspond (except the multiplication with the molecular volume or molecular area) to the chemical potentials in spatially homogeneous systems. Such homogeneous chemical potentials can in general be expressed as follows:

$$f'(\phi)\,\nu = \mu_0 + k_\mathrm{B}T\ln\left(\gamma(\phi)\,\frac{\phi^{1/n}}{1-\phi}\right)\,, \tag{16a}$$

$$f_s'(\phi_s)\,\nu_s = \mu_{s,0} + k_\mathrm{B}T\ln\left(\gamma_s(\phi_s)\,\frac{\phi_s^{1/n_s}}{1-\phi_s}\right)\,, \tag{16b}$$

where μ_0 and $\mu_{s,0}$ are reference chemical potentials, and k_B denotes the Boltzmann constant. Moreover, $\gamma(\phi)$ and $\gamma_s(\phi_s)$ are the volume and area fraction-dependent activity coefficients containing the components' interactions.

To highlight the role of such activity coefficients, we split up the free energies for bulk and surface, $f(\phi) = e(\phi) - s_\mathrm{mix}(\phi)T$ and $f_s(\phi_s) = e(\phi_s) - s_{\mathrm{mix},s}(\phi_s)T$, into the interaction free energy densities $e(\phi)$ and $e_s(\phi_s)$, and the mixing entropy densities, $s_\mathrm{mix} = -(k_\mathrm{B}/\nu)[(\phi/n)\ln\phi + (1-\phi)\ln(1-\phi)]$ and $s_{\mathrm{mix},s} = -(k_\mathrm{B}/\nu_s)[(\phi_s/n_s)\ln\phi_s + (1-\phi_s)\ln(1-\phi_s)]$ [31, 41, 42]. Here, the ratios of molecular volumes and areas between the molecule and the solvent are abbreviated by n for the bulk and n_s for the surface. Performing a viral expansion of the interaction free energy densities, $e = (k_\mathrm{B}T/\nu)[\omega\phi + \sum_{k=2}\chi(k)\phi^k]$ and $e_s = (k_\mathrm{B}T/\nu_s)[\omega_s\phi_s + \sum_{k=2}\chi_s(k)\phi_s^k]$, the reference chemical potentials are $\mu_0 = k_\mathrm{B}T(\omega + n^{-1} - 1)$ and $\mu_{s,0} = k_\mathrm{B}T(\omega_s + n_s^{-1} - 1)$. Here, ω and ω_s are the bulk and surface internal free energy, and $\chi(k)$ and $\chi_s(k)$ are viral expansion coefficients. Using the viral expansion, the activity coefficients can be expressed as

$$\gamma(\phi) = \exp\left(\sum_{k=2} k\,\chi(k)\,\phi^{k-1}\right)\,, \tag{17}$$

$$\gamma_s(\phi_s) = \exp\left(\sum_{k=2} k\,\chi_s(k)\,\phi_s^{k-1}\right)\,, \tag{18}$$

confirming that the activity coefficients depend exclusively on the components' interactions when introduced via equations (16).

We have seen that the contributions $\phi^{1/n}/(1-\phi)$ and $\phi_s^{1/n_s}/(1-\phi_s)$ in equations (16) stem from the respective mixing entropy. These contributions imply a scaling of the diffusive Onsager mobilities Λ and Λ_s with volume and area fractions, respectively. This scaling can be understood when considering the dilute limits in bulk and surface ($\phi \to 0$, $\phi_s \to 0$, and $\phi \to 1$, $\phi_s \to 1$). In these limits, the activity coefficients (defined via equations (16)) are $\gamma = 1$ and $\gamma_s = 1$, and the diffusion coefficients in bulk and surface, $D = k_\mathrm{B}T\Lambda f''$ and $D_s = k_\mathrm{B}T\Lambda_s f_s''$, have to be constants, i.e. independent of volume and area fractions. Thus, the mixing entropy implies the following scaling for the diffusive mobilities:

$$\Lambda = \Lambda_0\,\phi\,(1-\phi)\,, \tag{19a}$$

$$\Lambda_s = \Lambda_{s,0}\,\phi_s\,(1-\phi_s)\,, \tag{19b}$$

where Λ_0 and $\Lambda_{s,0}$ are mobility coefficients that can depend on volume and area fraction.

To tailor our model for phase separation in bulk and surface coupled via binding to a specific system, the activity coefficients for bulk $\gamma(\phi)$ and surface $\gamma_s(\phi_s)$, have to be chosen together with the coupling free energy density $J(\phi|_{z=0}, \phi_s)$. In section 3.1, we discuss a choice of such free energy densities to study the effects of surface binding on droplet spreading.

3. Wetting dynamics with surface binding

In this section, we investigate how the dynamics of the spreading of a droplet in the bulk is affected by surface binding and the possibility of phase separation in the surface. In this section, we consider a two-dimensional system with a one-dimensional boundary; see appendix E and figure 9 for the results considering a three-dimensional system with axial symmetry. using 2D numerical simulations. For such studies, we set for simplicity $\Lambda_{r\kappa} = 0$ and $\Lambda_\kappa = \Lambda_{\kappa_s} = \infty$, implying that the equilibrium boundary conditions equations (9b)–(9d) hold during the spreading dynamics. Moreover, we consider the mobility coefficients, Λ_0 and $\Lambda_{s,0}$, in equation (19a) to be constants, and the free energy cost $\kappa_0 = 0$, for simplicity.

3.1. Interaction free energies

To study spreading, we consider Flory-Huggins free energy densities for bulk and surface,

$$f(\phi) = \frac{k_\mathrm{B}T}{\nu}\left[\frac{1}{n}\phi\ln\phi + (1-\phi)\ln(1-\phi) - \chi\phi^2 + \omega\phi\right]\,, \tag{20a}$$

$$f_s(\phi_s) = \frac{k_\mathrm{B}T}{\nu_s}\left[\frac{1}{n_s}\phi_s\ln\phi_s + (1-\phi_s)\ln(1-\phi_s) - \chi_s\phi_s^2 + \omega_s\phi_s\right]\,. \tag{20b}$$

Using equation (16), the two free energies correspond to the activity coefficients, respectively:

$$\gamma(\phi) = \exp(-2\chi\phi)\,, \tag{20c}$$

$$\gamma_s(\phi_s) = \exp(-2\chi_s\phi_s)\,. \tag{20d}$$

In other words, we consider a mean-field free energy up to the second order, with the coefficients in the viral expansion $\chi(2) = -\chi$ and $\chi_s(2) = -\chi_s$.

Interactions between the surface and the bulk are captured by the coupling free energy density [16]:

$$J(\phi|_{z=0}, \phi_s) = \frac{k_\mathrm{B}T}{\nu_s}\left[\omega_0\,\phi|_{z=0} + \chi_{00}\,\phi|_{z=0}^2 + \chi_{0s}\,\phi|_{z=0}\,\phi_s\right]\,, \tag{20e}$$

which encompasses all relevant terms up to the second order. Note that a term proportional to ϕ_s^2 already exists in surface free energy density f_s (equation (20b)). In equation (20e), the parameter ω_0 represents the internal free energy of a bulk molecule at the surface. When the surface is attractive for bulk molecules, $\omega_0 < 0$. The coefficient χ_{00} quantifies the interactions among bulk molecules at the surface leading to enrichment ($\chi_{00} < 0$) or depletion ($\chi_{00} > 0$) at the surface. For simplicity, we have set χ_{00} to zero for the studies shown in this section. Furthermore, χ_{0s} describes the interactions between bound and unbound molecules at the surface. For all our studies, we have assigned a negative value to χ_{0s}. This choice corresponds to the case that molecules, bound or unbound, attract each other. For a comprehensive thermodynamic study of all three parameters, we refer the reader to [16].

3.2. Non-dimensionallization of dynamic equations and dimensionless parameters

To solve the dynamics equations, we write them in a dimension-less form. We obtain non-dimensional dynamic equations by rescaling length and time scales as follows:

$$\boldsymbol{x} \to \boldsymbol{x}\nu^{1/3}\,, \tag{21a}$$

$$t \to t\nu^{2/3}/(\Lambda_0 k_\mathrm{B}T)\,, \tag{21b}$$

$$\tilde{V} = \left\{ \boldsymbol{x}/\nu^{1/3} \, | \boldsymbol{x} \in V \right\} , \tag{21c}$$

$$\tilde{S} = \left\{ \boldsymbol{x}_{\parallel}/\nu^{1/3} \, | \boldsymbol{x}_{\parallel} \in S \right\} , \tag{21d}$$

where $\tilde{V}$ and $\tilde{S}$ are the rescaled bulk and surface. This choice leads to the following non-dimensional parameters:

$$\mathcal{D}_s = \frac{\Lambda_s}{\Lambda} , \tag{22a}$$

$$k_r = \Lambda_r \frac{\nu^{2/3}}{\Lambda_0} . \tag{22b}$$

Moreover, we introduce the following rescaled quantities: the rescaled bulk and surface free energy densities, $\tilde{f}(\phi) = (\nu/k_\mathrm{B}T)f(\phi)$ and $\tilde{f}_s(\phi_s) = (\nu/k_\mathrm{B}T)f_s(\phi_s)$, the rescaled coupling free energy density $\tilde{J}(\phi|_{z=0}, \phi_s) = (\nu_s/k_\mathrm{B}T)J(\phi_s, \phi|_{z=0})$, and the rescaled coefficients characterizing the free energy costs for gradients, $\tilde{\kappa} = \kappa\nu^{1/3}/(k_\mathrm{B}T)$, and $\tilde{\kappa}_s = (\nu_s/(k_\mathrm{B}T\nu^{2/3})\kappa_s$. The dimensionless equations governing the kinetics of the system are thus given as:

$$\partial_t \phi = \nabla \cdot \left[\phi\,(1-\phi) \left(\tilde{f}'' \nabla \phi - \tilde{\kappa} \nabla^3 \phi \right) \right] , \qquad \boldsymbol{x} \in \tilde{V}, \tag{23a}$$

$$\partial_t \phi_s = \nabla_{\parallel} \cdot \left[\mathcal{D}_s \phi_s\,(1-\phi_s) \left(\tilde{f}_s'' \nabla_{\parallel} \phi_s + \nabla_{\parallel} \frac{\partial \tilde{J}}{\partial \phi_s} - \tilde{\kappa}_s \nabla_{\parallel}^3 \phi_s \right) \right] + \tilde{r}\,(\phi_s, \phi|_{z=0}) , \qquad \boldsymbol{x} \in \tilde{S}. \tag{23b}$$

The dimensionless binding flux reads:

$$\tilde{r} = -k_r \left(\frac{\mu_s}{k_\mathrm{B}T} - \frac{\mu|_{z=0}}{k_\mathrm{B}T} \right) , \tag{23c}$$

with the chemical potential in bulk and surface,

$$\frac{\mu_s}{k_\mathrm{B}T} = \frac{\partial \tilde{f}_s}{\partial \phi_s} + \frac{\partial \tilde{J}}{\partial \phi_s} - \tilde{\kappa}_s \nabla_{\parallel}^2 \phi_s , \qquad \frac{\mu}{k_\mathrm{B}T} = \frac{\partial \tilde{f}}{\partial \phi} - \tilde{\kappa} \nabla^2 \phi . \tag{23d}$$

The boundary conditions in a dimensionless form are:

$$0 = \frac{\partial \tilde{J}}{\partial \phi|_0} + \frac{\nu_s}{\nu^{2/3}} \tilde{\kappa}\, \boldsymbol{n} \cdot (\nabla \phi)\,|_0 , \qquad \boldsymbol{x} \in \tilde{S}, \tag{23e}$$

$$0 = \tilde{\kappa}\, \boldsymbol{n} \cdot \nabla \phi , \qquad \boldsymbol{x} \in \partial\tilde{V}, \tag{23f}$$

$$0 = \tilde{\kappa}_s\, \boldsymbol{t} \cdot \nabla_{\parallel} \phi_s , \qquad \boldsymbol{x} \in \partial\tilde{S}, \tag{23g}$$

$$-\frac{\nu^{2/3}}{\nu_s} \tilde{r} = \phi\,(1-\phi)\, \boldsymbol{n} \cdot \nabla \frac{\mu}{k_\mathrm{B}T} , \qquad \boldsymbol{x} \in \tilde{S}, \tag{23h}$$

$$0 = \phi\,(1-\phi)\, \boldsymbol{n} \cdot \nabla \frac{\mu}{k_\mathrm{B}T} , \qquad \boldsymbol{x} \in \partial\tilde{V}. \tag{23i}$$

To numerically solve the dynamic equations (23), we develop a numerical solver for the corresponding systems of partial differential equations. Specifically, we employ the finite difference method for spatial discretization and the Crank–Nicolson scheme combined with the energy quadratization method [43–45] to discretize time.

3.3. Spreading kinetics towards complete wetting

We use our dynamic theory of wetting to investigate the influence of surface binding on the kinetics toward a completely wetted state. To this end, the system is initialized with a droplet near the surface where no molecules are initially bound (figures 1(b) and (c)). This initial droplet has local volume fractions corresponding to the equilibrium phase diagram. Such phase diagrams are, in general, determined by the interaction parameters χ, χ_s, and χ_{0s}. For simplicity, we choose equal molecular volumes and areas between molecule and solvent in bulk and surface, i.e. $n = 1$ and $n_s = 1$. We also fix $\chi_s = \chi = 2.5$ and $\chi_{0s} = -0.5$, and $N\nu/|V| = 0.17$ for the forthcoming studies ensuring that droplets are thermodynamically stable in bulk and surface; see appendix B for details. Moreover, refer to table 1 for a summary of the chosen parameter values for our wetting studies. For the sake of simplicity, the surface internal free energy ω_s has been assigned a value of zero. To describe repulsive interactions between the surface and bulk molecules, we choose $\omega_0 = 0.17$ in equation (20e), and we choose the interaction parameter of bulk molecules at the surface as $\chi_{00} = 0$.

To illustrate the qualitative behavior of the contact angle θ, we consider the wetting boundary condition equation (10), which is valid when the triple line is at local equilibrium. For the parameter choices discussed above, this condition gives $\cos(\theta) \propto -\partial J/\partial\phi = -(k_B T/\nu_s)[\omega_0 + \chi_{0s}\phi_s]$. We see that the contact angle varies with the area fraction of bound molecules. For our choices $\omega_0 > 0$ (repulsive) and $\chi_{0s} < 0$ (attractive), $\cos(\theta)(\phi_s = 0) < 0$, corresponding to partial wetting with $\pi/2 < \theta < \pi$ (for $\omega_0 = 0.17$), or the case of dewetting for even larger values of ω_0. When more molecules are bound to the surface ($\phi_s > 0$), $\cos(\theta)(\phi_s)$ increases linearly with a steeper slope for larger values of the surface-bulk coupling, $|\chi_{0s}|$. For large enough values of $|\chi_{0s}|$ and ϕ_s, the contact angle $\theta = 0$ corresponding to complete wetting. In summary, when more molecules are bound to the surface, the considered system tends to cross from partial wetting to complete wetting. As we initialize the system without molecules bound to the surface, we expect such a trend in wetting behavior upon surface binding.

For simplicity, we consider a two-dimensional domain for the bulk with a one-dimensional surface; see green line figure 2(a). In addition to the boundary conditions given in equations (23), periodic boundary conditions are applied along the left and right boundaries at ∂S and ∂V. An exception is the ∂V boundary opposite to the binding surface S where we apply no flux boundaries (non-binding), as stated in equation (1*d*).

3.3.1. Surface binding nucleates a surface droplet that accelerates spreading

After initializing the droplet adjacent to the surface, it develops a small bridge of molecule-rich phase with the surface; figure 2(a). As time progresses, the droplet slowly wets on the surface; figure 2(b). The dynamics is slow because the surface without binding is weakly repulsive ($\omega_0 > 0$). In the absence of binding, the droplet approaches a partially wetted state with a contact angle $\theta > \pi/2$. Note that without binding ($\phi_s = 0$), $\omega_0 = 0$ and $\chi_{00} = 0$ in equation (20*e*) leads to $J = 0$ and a contact angle of $\theta = \pi/2$ (equation (10)). However, molecules additionally start accumulating in the surface by binding. This accumulation is more pronounced right underneath the bulk droplet (figure 8(a) in appendix C). Once this local volume fraction exceeds the saturation volume fraction, a droplet gets nucleated inside the surface (figure 2(c)). This surface droplet grows quickly due to the influx of droplet material from the bulk droplet right above, indicated by the red arrow in the figure. As a result, the interface in the surface and the bulk coincide and start moving together (figure 2(d)). After that, the bulk droplet spreads quickly until it completely wets the surface (figures 2(e) and (f)). Concomitantly, the area fraction far away from the surface droplet reaches the equilibrium value from below (figure 8(b) in appendix C).

To characterize how the bulk droplet affects the lower dimensional surface droplet that had been nucleated via binding, we determine the contact area of the bulk droplet A on the surface and the area of the surface droplet A_s with time. As illustrated in figures 2(a)–(f), the area of the bulk droplet A first grows slowly. Suddenly, its growth speeds up quickly, leading to a completely wetted surface (figure 3(a)). The time at which the growth of the bulk droplet speeds up coincides with the time τ_n when a surface droplet is nucleated underneath the bulk droplet. Moreover, the time of fast spreading of the bulk droplet corresponds to the growth time τ_g of the surface droplet underneath, i.e. the time it takes for the surface droplet area A_s to grow from zero to full surface coverage.

Increasing the binding rate k_r to the surface speeds up both, nucleation and growth of surface droplets. This is evident by the shift of A and A_s to smaller times (figures 3(b) and (c)). The nucleation time τ_n and the growth time τ_g decays algebraically for smaller binding rate k_r, while both saturate for very large values of k_r. The saturation of both processes results from diffusion in bulk and membrane becoming rate limiting.

3.3.2. Incompatible phase equilibrium in bulk and surface

In our studies, the surface droplet grows until the surface is homogeneously covered by bound molecules. The absence of phase separation in the surface results from phase equilibria in bulk and surface being in general incompatible, except for very special parameter choices. Incompatible means that the condition for phase equilibrium in bulk ($\mu^{I} = \mu^{II}$) and surface ($\mu_s^{I} = \mu_s^{II}$) cannot be satisfied concomitantly.

To understand such incompatible equilibria for our coupled bulk-surface system, we first take a closer look at the free energy densities in bulk and surface, f and f_s; see figure 4(a) for a schematic sketch of f. For equal molecular volumes of molecule and solvent in the bulk ($n = 1$), the free energy density in the bulk f is a symmetric double-well potential (equation (20*a*)), where ϕ^{I} and ϕ^{II} are the equilibrium volume fractions in the molecule-rich and poor phase. In this case, the slope of the Maxwell construction corresponds to the bulk chemical potential $\mu = 0$. Though the surface free energy density f_s is also symmetric for $n_s = 1$ (equation (20*b*)), the total free energy density of the surface, $f_s + J$, is not symmetric when the interaction parameters ω_0, χ_{00} and χ_{0s} are non-zero in equation (20*e*). Since the coupling free energy density $J(\phi|_{z=0}^{I/II}, \phi_s)$ depends on the bulk phases right above, the total free energy density of the surface $(f_s + J)$ is different below the molecule-rich or molecule-poor phase, respectively (figures 4(b) and (c)). Since the coupling $\chi_{0s} < 0$ is

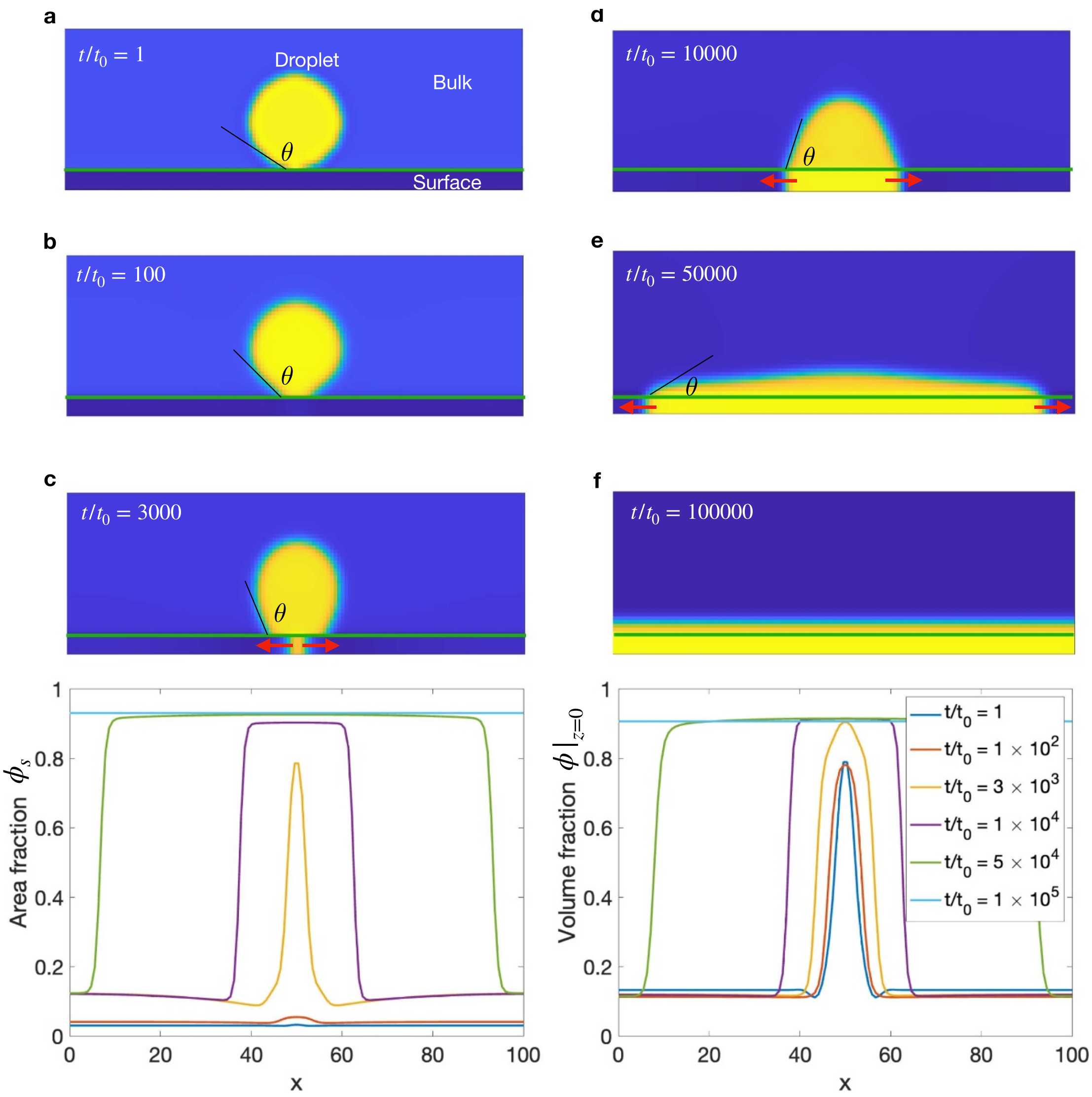

Figure 2. Bulk droplet spreading on a binding surface toward complete wetting. (a) Initially, the bulk droplet forms a bridge, and (b) slowly spreads on the surface (green line). (c) and (d) After nucleation of a surface droplet underneath the bulk droplet, (e) both droplet interfaces move synchronously, quickly covering the surface and finally leading to a completely wetted state (f). $\theta = 0^o$ at equilibrium. See appendix B for details. (g) and (h) show the surface-bound area fraction ϕ_s and boundary volume fraction of ϕ at $z = 0$, i.e. $\phi|_{z=0}$, of the snapshots in plot (a)–(f). Parameters: $k_r = 10^{-4}$, $\chi_{0s} = -0.5$, $t_0 = \nu^{2/3}/(\Lambda_0 k_B T)$, more see table 1. For all the numerical simulations in this study, we use $\Delta t = 10^{-1}$ and $\Delta x = 1/128$ as the temporal and spatial mesh size.

attractive, the Maxwell construction for phase coexistence in the surface would require that the surface chemical potential adjacent to the molecule-poor bulk phase, $\mu_s^{\mathrm{II}} < 0$. Since $\phi|_{z=0}^{\mathrm{I}} > \phi|_{z=0}^{\mathrm{II}}$, the Maxwell's slope $\mu_s^{\mathrm{I}} < 0$ is even more negative. As thermodynamic equilibrium also requires that binding equilibrium is satisfied (equation (9)), phase coexistence in bulk and surface is only possible if $\mu_s^{\mathrm{I}} = \mu^{\mathrm{I}} = 0$ and $\mu_s^{\mathrm{II}} = \mu^{\mathrm{II}} = 0$. These conditions cannot be satisfied in general; the only exception is when all three interaction parameters ω_0, χ_{00} and χ_{0s} vanish. If not, a bulk droplet can only coexist with a surface homogeneously covered by bound molecules. The equilibrium surface area fraction corresponds to the global minimum in the total surface free energy densities $(f_s + J)$ which is the surface molecule-rich phase in figure 4(c) (indicated by blue line).

3.3.3. Scaling of the nucleation time τ_{n}

The droplet phase is nucleated in the surface directly underneath the center position of the bulk droplet, $\boldsymbol{x}_{\|}|_{\mathrm{center}}$. Due to the mirror symmetry at this center position, lateral gradients have to vanish at the center in the bulk and surface ($\nabla_{\|}\phi_s = 0$ and $\nabla_{\|}\phi = 0$ at $\boldsymbol{x}_{\|}|_{\mathrm{center}}$). Consequently, the dynamic equation for the area fraction ϕ_s at the center positions reads

$$\partial_t \phi_s\big|_{\mathrm{center}} = k_r\left(\mu - \mu_{\mathrm{s}}\right)\big|_{\mathrm{center}}. \tag{24}$$

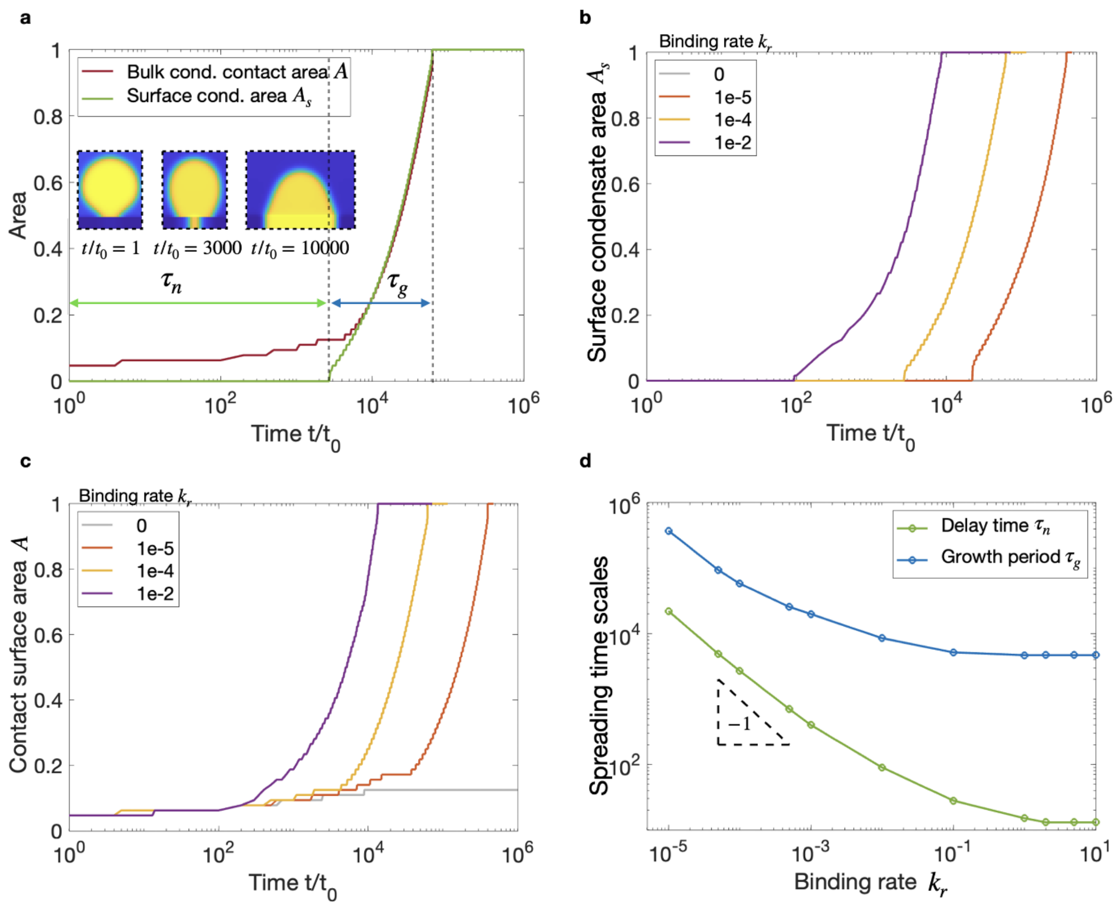

Figure 3. Spreading dynamics toward a completely wetted state is accelerated by surface binding. (a) The contact area of the bulk droplet A initially increases slowly while speeding up after the nucleation of a surface droplet around $t/t_0 = 3 \cdot 10^3$, evidenced by the fast increase of the surface droplet area A_s. The time once A_s is non-zero corresponds to the nucleation time τ_n of a surface droplet, and τ_g is the period for it to grow until it covers the full surface. (b) The area of the surface droplet A_s shows that the nucleation time τ_n decreases with increasing rescaled binding rate k_r. (c) The acceleration in the growth of the bulk droplet area shifts toward earlier times for increasing values of k_r. (d) The growth period τ_g and the nucleation time τ_n both scale proportional to k_r^{-1} for increasing rescaled binding rate k_r. For large values, diffusion in bulk and surface becomes rate-limiting, leading to a plateau. Parameters: $t_0 = \nu^{2/3}/(\Lambda_0 k_B T)$, more see table 1.

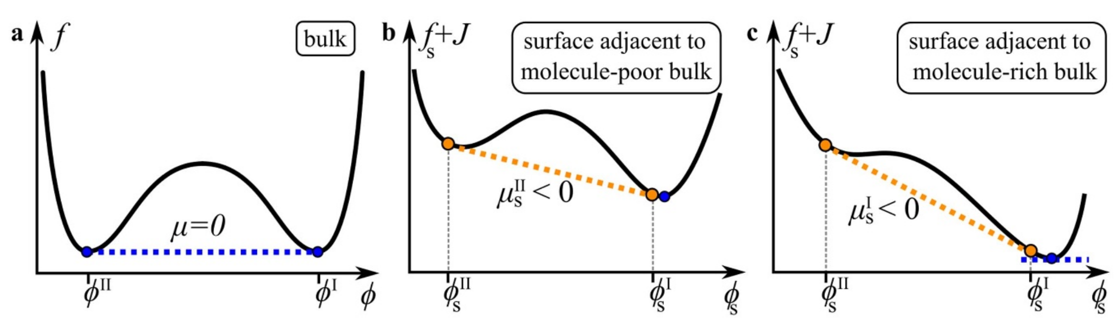

Figure 4. Incompatible phase equilibria in bulk and surface (a) The bulk free energy density f_s, where the Maxwell construction of the symmetric double well potential corresponds to a bulk chemical potential $\mu = 0$. (b) The total free energy density of the surface adjacent to a molecule-poor bulk phase, and (c) adjacent to a molecule-rich bulk phase. The Maxwell construction gives two different pairs of equilibrium area fractions, ϕ_s^{I} and ϕ_s^{II}. However, both cases are incompatible with phase equilibrium in the bulk, (a). In other words, thermodynamic equilibrium is a homogeneous state corresponding to the global minimum in (c).

Nucleation in the surface induced by the bulk droplet corresponds to the scenario where $\mu > \mu_s$ (figures 4(a)–(c)), i.e. molecules bind to the surface and nucleate a surface droplet when the local area fraction exceeds the equilibrium concentration (appendix B). If bulk diffusion is fast compared to binding ($k_r \ll 1$ in equation (22)), the bulk volume fractions inside and outside of the droplet are close to their respective equilibrium value at all times. This corresponds to a spatially constant μ at the moment of nucleation. This also implies that μ_s is spatially constant on the surface. Thus, the time to form a nucleus on the surface right beneath the center of the bulk droplet scales, $\tau_\mathrm{n} \sim \left(\partial_t \phi_s\big|_\mathrm{center}\right)^{-1} \simeq k_r^{-1}$. This scaling agrees with the result obtained from numerically solving the dynamics equations (23); see figure 3(d).

For fast binding compared to bulk diffusion ($k_r \gg 1$), nucleation of surface droplets is limited by diffusion in surface and bulk, while the binding is at equilibrium at all times, $\mu_s \simeq \mu$. Thus, the nucleation time τ_n becomes constant and independent of the binding rate k_r, which is consistent with the results in figure 3(d).

3.3.4. Scaling of the growth time τ_g for complete wetting

Now, we derive the scaling behavior of the growth time τ_g with the rescaled binding rate k_r. To this end, we first note that in the surface region underneath the droplet, the binding flux is negligible if the surface area fraction attains a value that correspond to a local chemical potential $\mu_s^\mathrm{I} = 0$. A sizable binding flux is hence limited to the surface region adjacent to the molecule-poor bulk phase, where we approximate the binding flux as $r = k_r \mu_s^\mathrm{II}$. In the following, we denote the position of the interface of the surface droplet by X_0. We note that in the case of complete wetting, the position of the droplet interface coincides with X_0 throughout the late stage of the spreading process (figures 2(d)–(f)). The time evolution of the average area fraction $\bar{\phi}_s$ (equation (4)) in rescaled units thus reads

$$\frac{\mathrm{d}\bar{\phi}_s}{\mathrm{d}t} = -2k_r \frac{\mu_s^\mathrm{II}}{k_\mathrm{B}T}\left(1 - \frac{X_0}{X_\mathrm{max}}\right), \tag{25}$$

where $X_\mathrm{max} = L/2$. In addition, volume conservation inside the surface implies:
$\bar{\phi}_s = 2\left(\phi_s^\mathrm{I} X_0 + \phi_s^\mathrm{II}(X_\mathrm{max} - X_0)\right)/X_\mathrm{max}$. Taking the time derivative gives

$$\frac{\mathrm{d}\bar{\phi}_s}{\mathrm{d}t} = 2\frac{\phi_s^\mathrm{I} - \phi_s^\mathrm{II}}{X_\mathrm{max}}\frac{\mathrm{d}X_0}{\mathrm{d}t}. \tag{26}$$

The interface speed of the surface droplet, $\mathrm{d}X_0/\mathrm{d}t$, is

$$\frac{\mathrm{d}X_0}{\mathrm{d}t} \simeq -k_\mathrm{r}\frac{\mu_s^\mathrm{II}}{k_\mathrm{B}T}(X_\mathrm{max} - X_0), \tag{27}$$

which implies that the growth time scales as $\tau_\mathrm{g} \sim k_r^{-1}$.

3.4. Spreading kinetics towards partial wetting

Now, we use our theory of wetting to investigate the influence of surface binding on the kinetics towards a partially wetted state. To this end, the system is initialized similarly as described in section 3.3, i.e. with a droplet near the surface at which no molecules are initially bound (figures 1(b) and (c)).

3.4.1. Surface binding controls the droplet partial wetting kinetics

To study the effects of binding on the spreading of a bulk droplet toward a partially wetted state, we reduced the attractive coupling between the bulk and surface, χ_{0s}, relative to the previous study towards complete wetting. Specifically, we choose $\chi_{0s} = -0.33$. The other parameters and boundary conditions remained the same as in the earlier study; see table 1.

The early dynamics is similar to spreading towards a completely wetted state (figures 5(a)–(d)): a bridge of dense phase forms from the bulk droplet, which spreads on the surface towards contact angle $\theta < \pi/2$. This is followed by a nucleation of a droplet in the surface which quickly grows due to binding from the bulk droplet. Due to the still attractive coupling interactive interactions χ_{00}, the contact angle of the bulk droplet and the surface increases.

The first difference to the case of complete wetting studied in section 3.3 occurs when the interface of the surface droplet aligns with the interface of the bulk droplet. Owing to the less attractive bulk-surface interaction, χ_{0s}, the bulk droplet can only partially wet the dense phase of the surface droplet. In fact, for time scales larger than the meeting time of both interfaces, t_o, the contact angle θ remains stationary and finite (figures 5(d)–(f)). For $t > \tau_\mathrm{o}$, the interface of the surface drop overtakes the interface of the bulk droplet. There is even a negative feedback: As the surface droplet approaches full surface coverage, the bulk droplet shrink at approximately fixed contact angle. This feedback arises because binding to the surface lowers the average volume fraction in the bulk. This effect vanishes when the bulk contains much more molecules than the surface, i.e. for macroscopic systems. However, such effect could be relevant for small system such as cellular compartments and small reaction containers used in system chemistry.

The area of the bulk droplet A and surface droplet A_s with time shift enable to quantitatively extract the overtaking time τ_o of both interfaces, in addition to the nucleation and growth time, τ_n and τ_g (figure 6(a)). The overtaking time τ_o corresponds to the intersection of A and A_s. For $t < \tau_\mathrm{n}$, the bulk droplet spreads

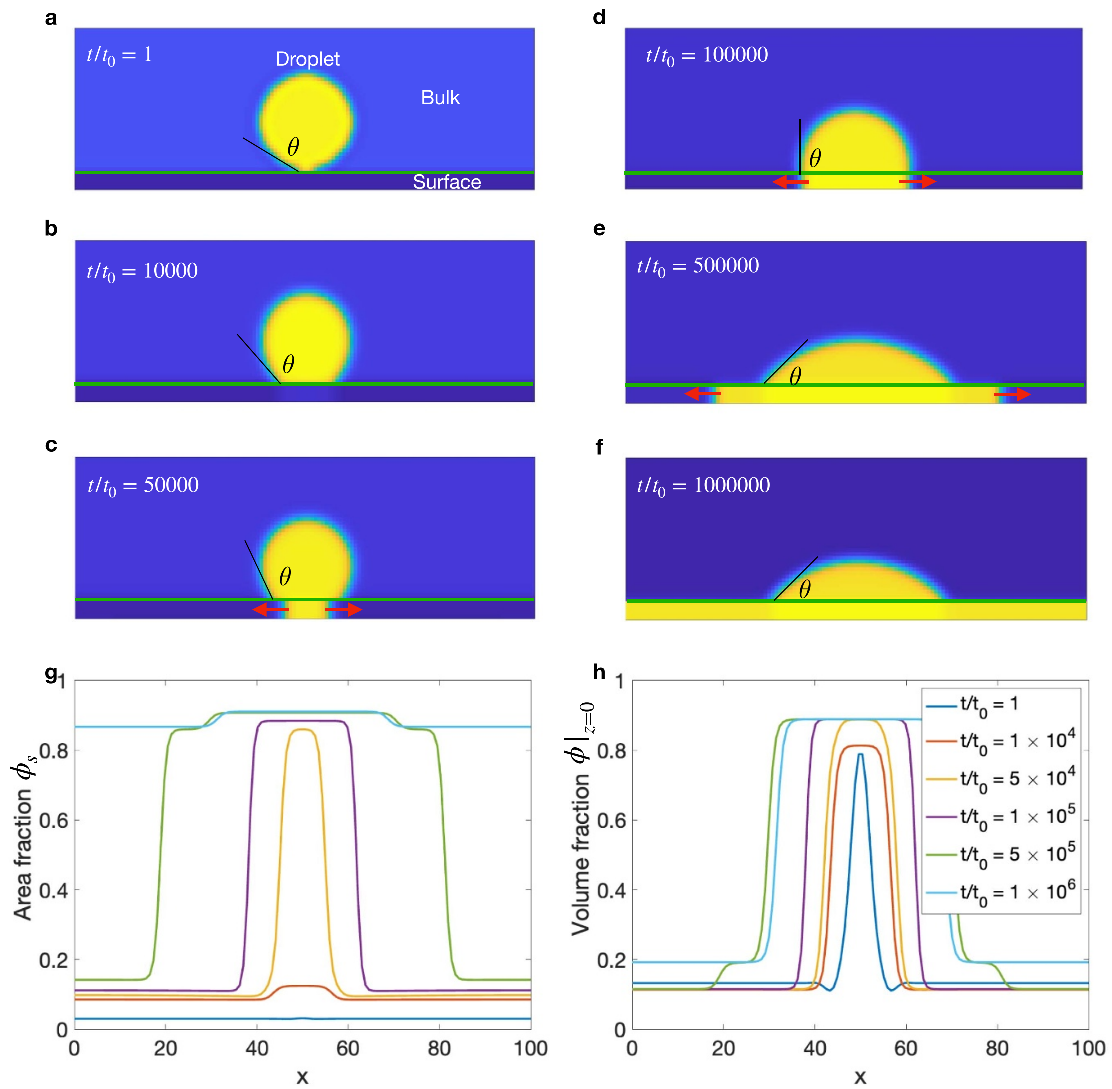

Figure 5. Bulk droplet spreading on a binding surface towards partial wetting. (a) After bridge formation, and (b) slow spreading on the surface (green line), (c) a surface droplet is nucleated. (d) and (e) The surface droplet grows and overtakes the interface of the bulk droplet, which arrests a constant contact angle θ. **f)** While the surface droplet grows towards a state that completely covers the surface, the bulk droplet shrinks a bit since the bulk loses molecules that bind to the surface. (g) and (h) show the surface-bound area fraction ϕ_s and boundary volume fraction of ϕ at $z = 0$, i.e. $\phi|_{z=0}$, of the snapshots in plot (a)–(f). Parameters: $k_r = 10^{-5}$, $\chi_{0s} = -0.33$, $t_0 = \nu^{2/3}/(\Lambda_0 k_B T)$, more see table 1. For all the numerical simulations in this study, we use $\Delta t = 10^{-1}$ and $\Delta x = L/128$ as the temporal and spatial mesh size.

essentially on the dilute phase, while for $\tau_n < t < \tau_o$, the bulk droplet spreads on a composition of dense and dilute phase on the surface. Finally, for $\tau_o < t < \tau_g$, the surface spreads inside the surface while the bulk droplet increases its contact a bit followed by a decrease to its equilibrium surface area.

Increasing the rescaled binding rate k_r shifts the contact area to shorter time scales (figure 6(b)). All three time scales, the nucleation time τ_n, the growth time τ_g and the overtaking time τ_o decrease algebraically proportional to κ_r^{-1} (figure 6(c)). For large values of κ_r, the three time scales are constant. Similar to the case of complete wetting, the reason is that diffusion in surface and bulk is rate limiting.

The contact angle θ with time shows a non-monotonous decrease toward the equilibrium value (figure 6(d)). While the contact angle decreases most times, it increases right after nucleation of the surface droplets. This effect stems from a transient depletion of ϕ_s underneath the bulk droplet interface. Depletion arises due to the diffusion of bound molecules toward the nucleated and growing surface droplet. According to local equilibrium at the triple line (equation (10)) and following the discussion at the beginning of section 3.3, a local decrease in ϕ_s underneath the bulk droplet interface increases the contact angle θ. In other words, this transient depletion due to the nucleation of the surface droplet effectively makes the surface a bit less attractive.

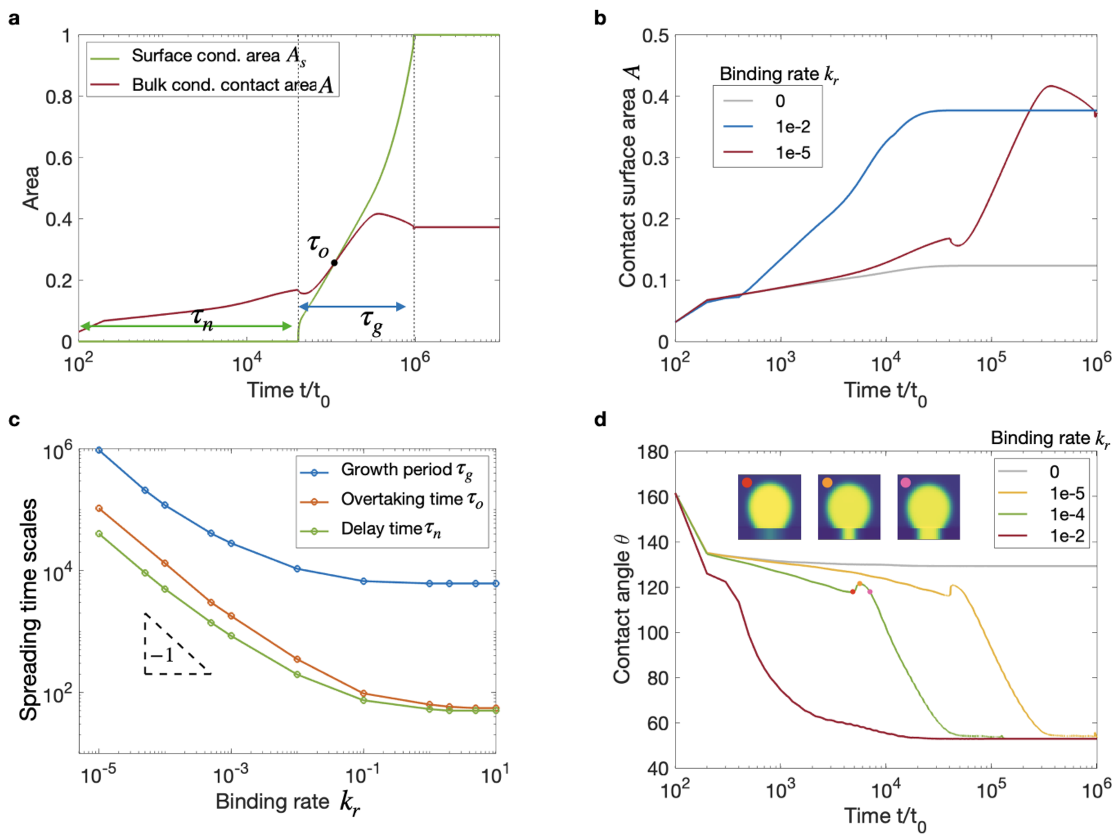

Figure 6. Spreading dynamics toward a partially wetted state is accelerated by surface binding. (a) The contact area of the bulk droplet A initially increases slowly until a surface droplet is nucleated at $t/t_0 = \tau_n$. The interface of the surface droplet takes over the interface of the bulk droplet at time τ_o and then quickly covers the full surface with a total growth time τ_g. In contrast, the bulk droplet stops spreading, leading to a constant contact angle θ and a slight shrinkage in drop volume due to the loss of bulk molecules by binding. (b) The area of the bulk droplet A shows that the spreading dynamics of the bulk droplet are more accelerated for faster rescaled binding rate k_r. (c) The growth period τ_g, the overtaking time τ_o and the nucleation time τ_n scale proportional to k_r^{-1} for increasing rescaled binding rate k_r. For large values in k_r, diffusion in bulk and surface becomes rate-limiting, leading to a plateau of all three quantities. (d) The contact angle θ has an initial decrease prior to the nucleation of a surface droplet. After its nucleation, there is significantly accelerated relaxation toward the partially wetted equilibrium state. There is a little hump in the time trace of θ, which arises from the spatial-temporal change of the surface the bulk droplet is wetting. Parameters: $t_0 = \nu^{2/3}/(\Lambda_0 k_B T)$, more see table 1.

3.4.2. Scaling of the growth time τ_g for partial wetting

To derive the scaling behavior for the growth time under complete wetting conditions, we start by noting the arguments leading to the time evolution $\mathrm{d}\bar{\phi}_s/\mathrm{d}t$ in equation (26) can be applied here as well (section 3.3.4). However, the relation between $\mathrm{d}\bar{\phi}_s/\mathrm{d}t$ and the binding flux need to be adjusted. Specifically, the position of the dense-dilute interface in the surface X_0 does not coincide with the droplet interface. We therefore introduce X_d to indicate the droplet interface position on the surface, where X_d itself is time dependent. The change of $\bar{\phi}_s$ over time thus reads

$$\frac{\mathrm{d}\bar{\phi}_s}{\mathrm{d}t} = -2k_r \frac{\mu_s^{\mathrm{II}}}{k_B T}\left(1 - \frac{X_d(t)}{X_{\max}}\right). \tag{28}$$

For fast binding $k_r \gg 1$, the time evolution of $X_d(t)$ is limited by diffusion in bulk and can be considered to be slow compared to the spreading dynamics in the surface. These considerations lead us to the scaling $\mathrm{d}X_0/\mathrm{d}t \sim k_r$ and $\tau_g \sim k_r^{-1}$ for the growth period.

4. Conclusions

Our research sheds light on a relatively unexplored facet of droplet spreading in the presence of surface binding. Using irreversible thermodynamics, we obtain the continuum equations for this wetting process and study the spreading of a droplet on a surface on which the droplet components can bind. A key finding is that binding controls the spreading dynamics toward a partially and a completely wetted thermodynamic equilibrium state. In particular, the spreading time scales with k_r^{-1}, where k_r is the binding rate to the surface. Spreading occurring on the characteristic time k_r^{-1} is a result of our consideration of small systems, i.e. a droplet spreading on a finite surface. Preliminary studies indicate that the spreading on larger surfaces is consistent with the expected power law behaviors [22, 23]. However, the verification of such slowly decaying power laws is difficult to investigate when numerically solving continuum equations as this requires system sizes and simulation times beyond currently available computational resources. Thus, we focus on the effects of surface binding on the spreading dynamics in smaller systems. A striking observation of our study is that binding creates a layer of droplet components on which spreading can be significantly accelerated. Acceleration is more pronounced if molecules remain attractive to each other after binding to the surface. This case leads to positive feedback on the wetting dynamics, which is more pronounced when more molecules are bound.

Our work describes a mechanism that is capable of controlling the wetting dynamics via the binding of molecules to surfaces. By manipulating the binding rates, we demonstrate control over the nucleation and growth rates of a droplet on the surface, which gives rise to accelerated wetting dynamics. There are other mechanisms that control wetting through changes of the surface properties, for example, adaptive wetting and reactive wetting.

We present a study on the wetting dynamics of a liquid droplet on a solid substrate, focusing on how the molecule-binding at the substrate surface increases the wettability of the substrate, thereby providing positive feedback for the wetting process. This situation is typical for systems undergoing reactive wetting [19, 20, 46–50] and adaptive wetting [21, 51, 52]. Reactive and adaptive wetting have been studied in systems where the substrate becomes either more or less wettable, or experiences alterations such as swelling, shrinking, or changes in surface chemistry. Our work studies a molecular mechanism of substrate properties effectively changing via molecular binding. This mechanism is fundamental in biological systems where proteins specifically bind receptors, altering the surface interactions with other molecules [53–55]. Such surface modifications are also relevant in non-biological systems, as studied in metallurgy, for example [56, 57]. Thus, our work may be a step towards a more unified description of complex wetting connecting the fields of reactive and adaptive wetting with biophysical systems composed of surface-binding biomolecules.

Wetting controlled via binding could be relevant for biomolecular condensates wetting membrane-bound organelles in living cells. For example, by enhancing the binding affinity of phase-separating proteins (phosphorylation, etc), the wetting propensity of biomolecular condensates and their spreading speed can be accelerated by nucleating a condensate of bound proteins on the organelle surface. An exciting layer of complexity emerges because intracellular membranes can vary significantly in their curvature. While a membrane interaction with a small droplet can always be approximated as a flat surface, we expect membrane curvature to become more relevant with increasing droplet size. Strikingly, condensates are expected to wet with a smaller contact angle or even completely wet the organelles if the condensate components can bind specifically to that organelle. Such a binding-mediated control mechanism could be crucial in regulating the communication between biomolecular condensates and membrane-bound organelles through specific feedback loops.

Future theoretical investigations should be concerned with the role of hydrodynamics during the spreading dynamics with surface binding [58, 59]. An interesting related question is whether the binding layer is an example of the thin surface film preceding the wetting dynamics, often called precursor film [22, 25–28]. Future research will delve into pattern formation on surfaces in bulk-surface systems driven by fuel-driven binding cycles [31, 60].

Data availability statement

All data that support the findings of this study are included within the article (and any supplementary files).

Acknowledgments

We thank all the anonymous reviewers for very constructive feedback on the manuscript. We thank S Gomez for carefully reading our manuscript and giving feedback, and G Granatelli for improving the illustration (figure 1). We thank G Bartolucci, J Bauermann, L Hubatsch, S Bo, S Laha, T Harmon, I LuValle-Burke, and D Sun for insightful discussions. We thank David Zwicker for his valuable comments on calculating contact angles. X Zhao acknowledges the 'FoSE New Researchers Grant' of the University of Nottingham Ningbo China for financial support. A Honigmann and C Weber acknowledge the SPP 2191 'Molecular Mechanisms of Functional Phase Separation' of the German Science Foundation for financial support and for providing an excellent collaborative environment.

Conflicts of interest

There are no conflicts to declare.

Appendix A. Derivation of binding flux

In this section, we derive the relationship (equation (1*c*)) between the surface diffusion flux $\boldsymbol{j}_s$ and the binding flux r. Taking the time derivative of the conserved particle number N (equation (2), and $\mathrm{d}N/\mathrm{d}t = 0$), we get

$$0 = \int_S \mathrm{d}S \left(\frac{\partial \phi_s}{\partial t}\right)/\nu_s + \int_V \mathrm{d}V \left(\frac{\partial \phi}{\partial t}\right)/\nu\,. \tag{A1}$$

Using the conservation laws (equations (1)) and the divergence theorem,

$$0 = \int_S \mathrm{d}S\,(r/\nu_s - \boldsymbol{n}\cdot\boldsymbol{j}/\nu) - \int_{\partial V} \mathrm{d}S\,\boldsymbol{n}\cdot\boldsymbol{j}/\nu - \int_{\partial S} \mathrm{d}l\,\boldsymbol{t}\cdot\boldsymbol{j}_s/\nu_s\,. \tag{A2}$$

This condition is fulfilled when equation (1*c*) is satisfied, together with equation (1*d*). For ∂S, we consider periodic boundary conditions.

Appendix B. Initialization of wetting studies and equilibrium contact angle for partial and complete wetting

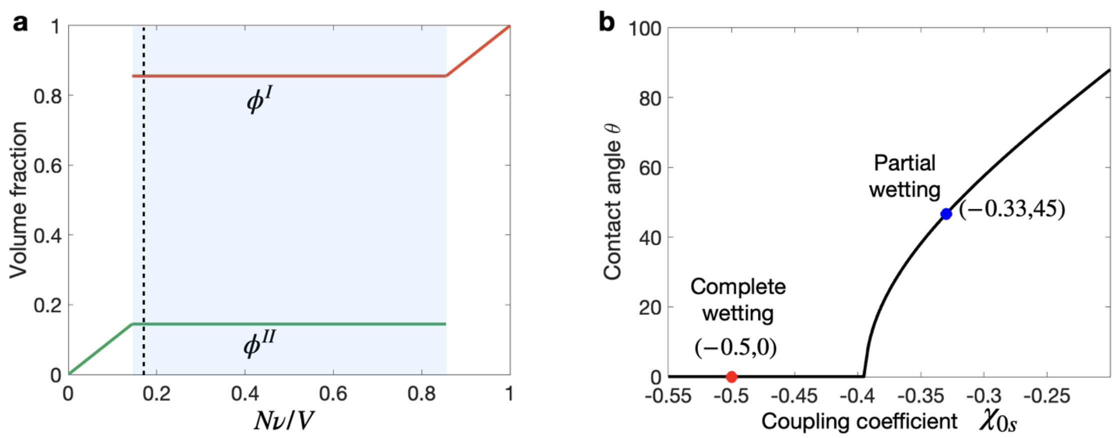

Figure 7. Parameter initialization in the numerical simulations. (a) To study the wetting dynamics, a bulk droplet is initialized with a volume V^{I} and volume fractions in the molecule-rich (I) and molecule-poor (II) phase corresponding to the phase diagram without binding ($\phi_s = 0$). For all studies, the conserved total volume fraction is $N\nu/|V| = 0.17$, which is indicated by the vertical dashed line. (b) The wetting dynamics approaches thermodynamic equilibrium with an equilibrium contact angle θ. This value is determined by the interaction parameter between bulk and surface, χ_{0s}. We consider two cases: relaxation toward a completely wetted state ($\chi_{0s} = -0.5$) and a partially wetted state ($\chi_{0s} = -0.33$). We note that we calculate the equilibrium values for ϕ_s, ϕ with respect to difference interaction parameter strength χ_{0s} using the equilibrium conditions in an ensemble where the chemical potential μ is fixed (see details in [16]). The contact angle θ is obtained by the law of Young–Dupré at equilibrium.

For all wetting studies, a single bulk droplet is initialized right on top of the surface where no molecules are initially bound ($\phi_s(\boldsymbol{x}_\parallel, t=0) = 0$). The volume fractions inside (I) (molecule-rich phase) and outside (II) (molecule-poor phase) are chosen to be homogeneous at $t = 0$ and in accordance with the equilibrium volume fractions in the absence of surface binding, ϕ^{I} and ϕ^{II} (figure 7(a)). Moreover, at $t = 0$, we also use the equilibrium value for bulk droplet volume, $V^{\mathrm{I}}(t=0) = (N\nu - \phi^{\mathrm{II}})/(\phi^{\mathrm{I}} - \phi^{\mathrm{II}})$. Note that for all studies, the conserved total volume fraction is $N\nu/|V| = 0.17$. The position of the droplet center is chosen such that wetting dynamics get initiated by the bridge formation of a molecule-rich phase in the absence of fluctuations.

At large times, the wetting dynamics reaches the corresponding thermodynamic equilibrium state. In our work, we studied the dynamics towards to completely wetted state (section 3.3) and a partially wetted state (section 3.4). For both cases, the used parameters are given in table 1, except the interaction parameter between bulk and surface, χ_{0s}. The more negative this parameter, the stronger the attraction between bound molecules and the bulk molecules adjacent to the surface. In other words, decreasing χ_{0s} towards more negative values leads to a transition between a partially wetted to a completely wetted equilibrium state (figure 7(b)). For our studies, we employ $\chi_{0s} = -0.5$ leading to a completely wetted state with a contact angle $\theta = 0$ and a homogeneous surface area fraction $\phi_s = 0.9717$ at thermodynamic equilibrium. For $\chi_{0s} = -0.33$, the bulk droplet partially wets the surface. The corresponding equilibrium contact angle $\theta \simeq \pi/4$ and the surface area fraction is slightly different underneath the molecule-rich (I) ($\phi_s = 0.9156$) and molecule-poor bulk phase (II) ($\phi_s = 0.8769$). We note that we calculate the equilibrium values for ϕ_s with respect to difference interaction parameter strength χ_{0s} using the equilibrium conditions in an ensemble where the chemical potential μ is fixed (see details in [16]). The contact angle θ is obtained by the law of Young–Dupré.

Appendix C. Nucleation of surface droplet by bulk droplet

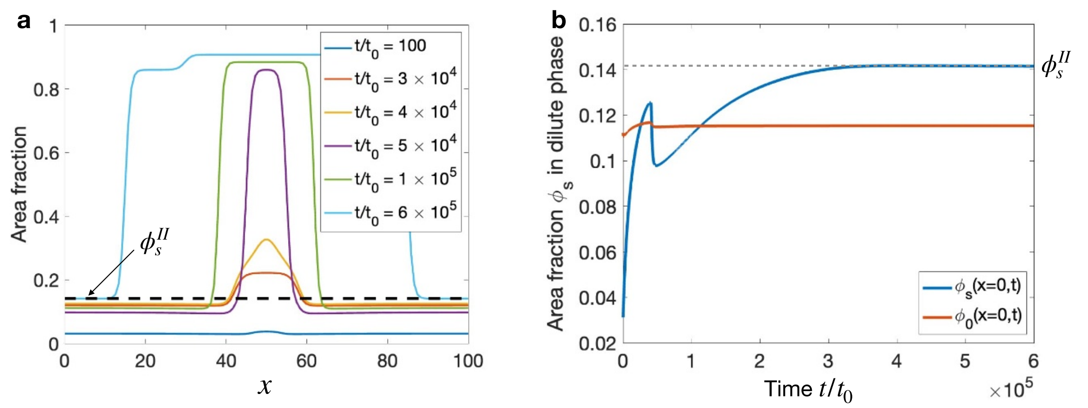

Figure 8. Heterogeneous nucleation of a surface droplet induced by a bulk droplet situated on top of the surface. (a) The area fraction ϕ_s of surface-bound molecules increases and peaks below the center of the bulk droplet due to the heterogeneous surface binding. Once this peak area fraction exceeds the equilibrium value ϕ_s^{II} (black dash line, sketch see figure 4(c), a droplet at the surface center is nucleated. (b) The surface-bound area fraction ϕ_s (blue solid line) and the bulk volume fraction at the bottom boundary $\phi|_{z=0}$ in the dilute phase change non-linearly. Initially, the nucleation of a surface droplet at the center leads to a decrease in the area fraction value far from the center. On longer times, the area fraction ϕ_s far from the surface droplet at $x = 0$ approaches the equilibrium area fraction ϕ_s^{II} (dashed line in plot (a)) from below. The bulk volume fraction at the surface $\phi|_{z=0}(x = 0, t)$ shows a similar as the area fraction of the bound molecules $\phi_s(x = 0, t)$ but with less magnitude variation due to the attractive coupling between $\phi_s(x = 0, t)$ and $\phi|_{z=0}(x = 0, t)$. We note that when the interface of the surface droplet reaches the system size, there is a sudden increase in the area fraction to the thermodynamic equilibrium value (dense phase, not shown). For both figures, $\chi_{0s} = -0.33$. Further parameter values are listed in table 1.

After bridge formation on the slightly repulsive surface ($\omega_0 > 0$), the binding of molecules from the bulk to the surface enhances the wetting propensity of the bulk droplet. Binding makes the surface effectively more attractive through the interactions between bound molecules and bulk molecules adjacent to the surface ($\chi_{0s} < 0$). Interestingly, the increase of bound molecules is more pronounced underneath the center of the bulk droplet (figure 8(a)). Once the local area fraction ϕ_s exceeds the equilibrium area fraction $\phi_s^{\mathrm{II}} = 0.1415$ (sketch see figure 4(c), a surface droplet gets nucleated. Note that only the position centered underneath the bulk droplet crosses the equilibrium value ϕ_s^{II}, while the surface domain far away and closer to the boundaries remains undersaturated. The corresponding area fractions far away from the surface droplet approach ϕ_s^{II} from below (figure 8(b)). This study shows that the bulk droplet indeed nucleates the formation of a droplet on the surface.

Appendix D. Parameters used for wetting studies

In our wetting studies, we consider two values of the interaction parameter between bulk and surface $\chi_{0s} = \{-0.5, -0.33\}$, corresponding to the cases where the system approaches complete or partial wetting at thermodynamic equilibrium. We also vary the dimensionless binding rate k_r (definition see equation (22)). The remaining parameters are kept fixed for all presented studies. Such parameters are summarized in table 1.

Table 1. Model parameters and their dimensionless values considered for the studies on wetting dynamics.

Parameter name	Symbol	rescaled value
Interaction coefficient at the surface	χ_s	2.5
Interaction coefficient in bulk	χ	2.5
Binding energy per unit area	ω_0	0.17
Internal free energy coefficient of molecule in the bulk	ω	2.5
Internal free energy coefficient of molecules at the surface	ω_s	2.5
Interaction coefficient accumulating at the surface	χ_{00}	0
Diffusion coefficient in the membrane	D_s	1
Gradient coefficient of molecule in the membrane	κ_s	1
Gradient coefficient of molecule in the bulk	κ	1
Domain size of the bulk	$L_x \times L_y$	100×30

Appendix E. Numerical study in three-dimensional cylindrical coordinates with axial symmetry

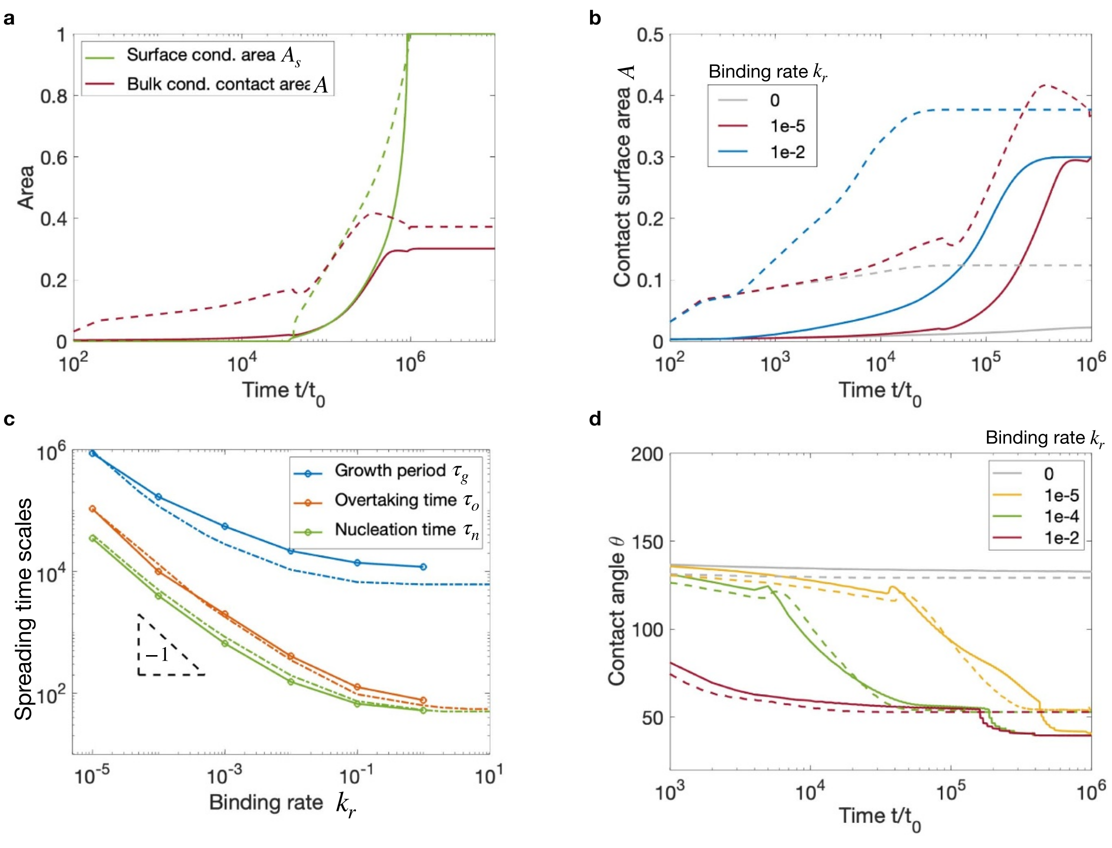

Figure 9. Spreading dynamics towards a partially wetted state in three-dimensional cylindrical coordinates with rotational symmetry (axial symmetric case). In all the plots presented here, solid lines denote the results in three-dimensional (3D) cylindrical coordinates and dashed lines the referenced results in two-dimensional (2D) Cartesian coordinates (see figure 6). (a) and (b) compare the contact area of the bulk droplet and the area of the surface droplet between 2D and 3D, illustrating how dimensionality affects the spreading behavior. (c) 2D and 3D studies give almost the same spreading time scales (τ_g, τ_o, τ_n). (d) We find a similar dynamic behavior between 2D and 3D but different equilibrium profiles in contact angle θ.

To explore whether the qualitative results for the planar setting are still valid in three dimensions (3D), we consider a rotational symmetric problem in cylindrical coordinates. The Laplace operator in cylindrical coordinates for a axial symmetric system reads:

$$\Delta = \mathrm{d}^2/\mathrm{d}r^2 + (1/r)\,\mathrm{d}/\mathrm{d}r + \mathrm{d}^2/\mathrm{d}z^2. \tag{E1}$$

We repeat the numerical calculations with the parameter values in section 3.4.1, and compare the results with the ones in two dimensional (2D) Cartesian coordinates (see figure 9 for details). We found that 2D and 3D studies share almost same spreading time scales (τ_g, τ_o, τ_n; see figure 9(c) and similar dynamic behavior in contact angle θ, but with notable differences in the equilibrium profiles (figure 9(d)), as well as in the bulk droplet contact area A at equilibrium (figures 9(a) and (b)). Still, these results indicate that qualitative results for the spreading dynamics with surface binding are robust between two and three-dimensional domains.

ORCID iDs

Xueping Zhao https://orcid.org/0000-0002-8679-6032
Susanne Liese https://orcid.org/0000-0001-7420-5488
Frank Jülicher https://orcid.org/0000-0003-4731-9185
Christoph A Weber https://orcid.org/0000-0001-6279-0405

References

[1] Boisvert F M, van Koningsbruggen S, Navascués J and Lamond A I 2007 The multifunctional nucleolus *Nat. Rev. Mol. Cell Biol.* **8** 574–85
[2] Friedman J R and Nunnari J 2014 Mitochondrial form and function *Nature* **505** 335–43
[3] Luzio J P, Pryor P R and Bright N A 2007 Lysosomes: fusion and function *Nat. Rev. Mol. Cell Biol.* **8** 622–32
[4] Brangwynne C P, Mitchison T J and Hyman A A 2011 Active liquid-like behavior of nucleoli determines their size and shape in xenopus laevis oocytes *Proc. Natl Acad. Sci.* **108** 4334–9
[5] Mahen R and Venkitaraman A R 2012 Pattern formation in centrosome assembly *Curr. Opin. Cell Biol.* **24** 14–23
[6] Gall J G 2003 The centennial of the cajal body *Nat. Rev. Mol. Cell Biol.* **4** 975–80
[7] Brangwynne C P, Eckmann C R, Courson D S, Rybarska A, Hoege C, Gharakhani J, Jülicher F and Hyman A A 2009 Germline p granules are liquid droplets that localize by controlled dissolution/condensation *Science* **324** 1729–32
[8] Fritsch A W, Diaz-Delgadillo A F, Adame-Arana O, Hoege C, Mittasch M, Kreysing M, Leaver M, Hyman A A, Jülicher F and Weber C A 2021 Local thermodynamics govern formation and dissolution of caenorhabditis elegans p granule condensates *Proc. Natl Acad. Sci.* **118** e2102772118
[9] Buchan J R and Parker R 2009 Eukaryotic stress granules: the ins and outs of translation *Mol. Cell* **36** 932–41
[10] Decker C J and Parker R 2012 P-bodies and stress granules: possible roles in the control of translation and mRNA degradation *Cold Spring Harbor Perspect. Biol.* **4** a012286
[11] Ma W and Mayr C 2018 A membraneless organelle associated with the endoplasmic reticulum enables 3'utr-mediated protein-protein interactions *Cell* **175** 1492–506
[12] Goehring N W, Trong P K, Bois J S, Chowdhury D, Nicola E M, Hyman A A and Grill S W 2011 Polarization of par proteins by advective triggering of a pattern-forming system *Science* **334** 1137–41
[13] Hubatsch L, Peglion F, Reich J D, Rodrigues N T L, Hirani N, Illukkumbura R and Goehring N W 2019 A cell-size threshold limits cell polarity and asymmetric division potential *Nat. Phys.* **15** 1078–85
[14] Ramm B, Heermann T and Schwille P 2019 The E. coli mincde system in the regulation of protein patterns and gradients *Cell. Mol. Life Sci.* **76** 4245–73
[15] Zacharogianni M, Aguilera-Gomez A, Veenendaal T, Smout J and Rabouille C 2014 A stress assembly that confers cell viability by preserving eres components during amino-acid starvation *eLife* **3** e04132
[16] Zhao X, Bartolucci G, Honigmann A, Jülicher F and Weber C A 2021 Thermodynamics of wetting, prewetting and surface phase transitions with surface binding *New J. Phys.* **23** 123003
[17] Rouches M, Veatch S L and Machta B B 2021 Surface densities prewet a near-critical membrane *Proc. Natl Acad. Sci.* **118** 290a
[18] Jülicher F and Weber C A 2024 Droplet physics and intracellular phase separation *Annu. Rev. Condens. Matter Phys.* **15** 237–61
[19] Kumar G and Prabhu K N 2007 Review of non-reactive and reactive wetting of liquids on surfaces *Adv. Colloid Interface Sci.* **133** 61–89
[20] Eustathopoulos N and Voytovych R 2016 The role of reactivity in wetting by liquid metals: a review *J. Mater. Sci.* **51** 425–37
[21] Butt H J, Berger R, Steffen W, Vollmer D and Weber S A L 2018 Adaptive wetting-adaptation in wetting *Langmuir* **34** 11292–304
[22] Brochard F and de Gennes P-G 1984 Spreading laws for liquid polymer droplets : interpretation of the "foot" *J. Phys. Lett.* **45** 597–602
[23] de Gennes P-G, Brochard-Wyart F and Quéré D 2004 *Capillarity and Wetting Phenomena: Drops, Bubbles, Pearls, Waves* (Springer)
[24] Cormier S L, McGraw J D, Salez T, Raphaël E and Dalnoki-Veress K 2012 Beyond tanner's law: crossover between spreading regimes of a viscous droplet on an identical film *Phys. Rev. Lett.* **109** 154501
[25] Hardy W 1919 The spreading of fluids on glass *Phil. Mag.* **38** 49–55
[26] Leger L, Erman M, Guinet-Picard A M, Ausserre D and Strazielle C 1988 Precursor film profiles of spreading liquid drops *Phys. Rev. Lett.* **60** 2390–93
[27] Xu H, Shirvanyants D, Beers K, Matyjaszewski K, Rubinstein M and Sheiko S S 2004 Molecular motion in a spreading precursor film *Phys. Rev. Lett.* **93** 206103
[28] Popescu M N, Oshanin G, Dietrich S and Cazabat A-M 2012 Precursor films in wetting phenomena *J. Phys.: Condens. Matter* **24** 243102
[29] Su W-C, Ho J C S, Gettel D L, Rowland A T, Keating C D , Parikh A N 2024 Kinetic control of shape deformations and membrane phase separation inside giant vesicles *Nat. Chem.* **16** 54–62
[30] Liese S, Zhao X, Weber C A and Jülicher F 2023 Chemically active wetting (arXiv:2312.07239)
[31] Weber C A, Zwicker D, Jülicher F and Lee C F 2019 Physics of active emulsions *Rep. Prog. Phys.* **82** 064601
[32] Young T 1805 III. An essay on the cohesion of fluids *Phil. Trans. R. Soc.* **95** 65–87
[33] Dupré A and Dupré P 1869 *Théorie Mécanique de la Chaleur* (Gauthier-Villars)
[34] de Gennes P-G 1985 Wetting: statics and dynamics *Rev. Mod. Phys.* **57** 827–63
[35] Jülicher F and Prost J 2009 Generic theory of colloidal transport *Eur. Phys. J.* E **29** 27–36
[36] De Groot S R and Mazur P 2013 *Non-Equilibrium Thermodynamics* (Courier Corporation)
[37] Livi R and Politi P 2017 *Nonequilibrium Statistical Physics: a Modern Perspective* (Cambridge University Press)

[38] Fischer H P, Maass P and Dieterich W 1997 Novel surface modes in spinodal decomposition *Phys. Rev. Lett.* **79** 893–6
[39] Fischer H P, Maass P and Dieterich W 1998 Diverging time and length scales of spinodal decomposition modes in thin films *Europhys. Lett.* **42** 49
[40] Kenzler R, Eurich F, Maass P, Rinn B, Schropp J, Bohl E and Dieterich W 2001 Phase separation in confined geometries: Solving the cahn–hilliard equation with generic boundary conditions *Comput. Phys. Commun.* **133** 139–57
[41] Flory P J 1942 Thermodynamics of high polymer solutions *J. Chem. Phys.* **10** 51–61
[42] Huggins M L 1942 Some properties of solutions of long-chain compounds *J. Phys. Chem.* **46** 151–8
[43] Zhao J, Yang X, Gong Y, Zhao X, Yang X, Li J and Wang Q 2018 A general strategy for numerical approximations of non-equilibrium models-part I: thermodynamical systems *Int. J. Numer. Anal. Model.* **15** 884–918 (available at: http://global-sci.org/intro/article_detail/ijnam/12613.html)
[44] Zhao J, Yang X, Li J and Wang Q 2016 Energy stable numerical schemes for a hydrodynamic model of nematic liquid crystals *SIAM J. Sci. Comput.* **38** A3264–90
[45] Zhao X and Wang Q 2019 A second order fully-discrete linear energy stable scheme for a binary compressible viscous fluid model *J. Comput. Phys.* **395** 382–409
[46] Zheng D W, Wen W and Tu K N 1998 Reactive wetting- and dewetting-induced diffusion-limited aggregation *Phys. Rev.* E **57** R3719–22
[47] Eustathopoulos N, Garandet J P, Drevet B, Eustathopoulos N, Garandet J P, Drevet B, Hondros E D, McLean M and Mills K C 1998 Influence of reactive solute transport on spreading kinetics of alloy droplets on ceramic surfaces *Phil. Trans. R. Soc.* A **356** 871–84
[48] Sumino Y, Kitahata H, Yoshikawa K, Nagayama M, Nomura S M, Magome N and Mori Y 2005 Chemosensitive running droplet *Phys. Rev.* E **72** 041603
[49] Sumino Y, Magome N, Hamada T and Yoshikawa K 2005 Self-running droplet: emergence of regular motion from nonequilibrium noise *Phys. Rev. Lett.* **94** 068301
[50] John K, Bär M and Thiele U 2005 Self-propelled running droplets on solid substrates driven by chemical reactions *Eur. Phys. J.* E **18** 183–99
[51] Hartmann S, Diekmann J, Greve D and Thiele U 2024 Drops on polymer brushes: advances in thin-film modeling of adaptive substrates *Langmuir* **40** 4001–21
[52] Kap O, Hartmann S, Hoek H, de Beer S, Siretanu I, Thiele U and Mugele F 2023 Nonequilibrium configurations of swelling polymer brush layers induced by spreading drops of weakly volatile oil *J. Chem. Phys.* **158** 174903
[53] Pombo-García K, Adame-Arana O, Martin-Lemaitre C, Jülicher F and Honigmann A 2024 Membrane prewetting by condensates promotes tight-junction belt formation *Nature* **632** 647–55
[54] Moser M, Legate K R, Zent R and Fässler R 2009 The tail of integrins, talin and kindlins *Science* **324** 895–9
[55] Harrington L, Fletcher J, Heermann T, Woolfson D and Schwille P 2021 De novo design of a reversible phosphorylation-dependent switch for membrane targeting *Nat. Commun.* **12** 1472
[56] Orejon D, Oh J, Preston D J, Yan X, Sett S, Takata Y, Miljkovic N and Sefiane K 2024 Ambient-mediated wetting on smooth surfaces *Adv. Colloid Interface Sci.* **324** 103075
[57] Chobaomsup V, Metzner M and Boonyongmaneerat Y 2020 Superhydrophobic surface modification for corrosion protection of metals and alloys *J. Coat. Technol. Res.* **17** 583–93
[58] Anderson D M, McFadden G B and Wheeler A A 1998 Diffuse-interface methods in fluid mechanics *Annu. Rev. Fluid Mech.* **30** 139–65
[59] Yue P, Zhou C and Feng J J 2010 Sharp-interface limit of the cahn–hilliard model for moving contact lines *J. Fluid Mech.* **645** 279–94
[60] Bartolucci G, Adame-Arana O, Zhao X and Weber C A 2021 Controlling composition of coexisting phases via molecular transitions *Biophys. J.* **120** 4682–97